J. Fluid Mech. (2013), *vol.* 733, *pp.* 268–301. © Cambridge University Press 2013
doi:10.1017/jfm.2013.442

A nonlinear model for indirect combustion noise through a compact nozzle

Maxime Huet† and Alexis Giauque

ONERA – The French Aerospace Lab, F-92322 Châtillon, France

(Received 6 March 2013; revised 26 June 2013; accepted 19 August 2013;
first published online 23 September 2013)

The present paper deals with the generation of sound by the passage of acoustic or entropy perturbations through a nozzle in the nonlinear regime and in the low-frequency limit. The analytical model of Marble and Candel for compact nozzles (*J. Sound Vib.*, vol. 55, 1977, pp. 225–243), initially developed for excitations in the linear regime, is rederived and extended to the nonlinear domain. Full nonlinear and second-order models are written for both subcritical and supercritical nozzles in the absence of shock and a detailed methodology is provided for the resolution of the second-order system. The accuracy of the second-order model is assessed for entropy forcings. It is shown to be accurate for all waves, with the exception of the upstream generated wave for subcritical diverging geometries where higher-order nonlinear contributions cannot be neglected. In the context of indirect combustion noise, the phenomenon of regime change of the nozzle due to an incoming entropy fluctuation is also addressed. Regime change is related to a Mach number modification induced by temperature and velocity fluctuations. In the present study, it translates into a limitation of the maximum amplitude of the incoming entropy forcing. Such limitations are to be considered for subcritical nozzles with significant inlet or outlet Mach numbers, where the flow transition is observed even for very low-amplitude entropy excitations. With the constraint of those limitations, the analytical extended nozzle describing functions representing the full nonlinear response for indirect combustion noise are validated through detailed comparisons with numerical simulations.

Key words: acoustics, aeroacoustics

1. Introduction

The large efforts performed over the last decades to reduce the main noise sources of aircraft, especially jet and fan noise, led to the relative increase of other acoustic sources that were previously considered negligible. The amplitude of these contributions, such as engine core noise, should be also reduced if the objectives of the ACARE (Advisory Council for Aviation Research and innovation in Europe) for 2020 are to be met (ACARE 2010). Among those noise sources, the one resulting from combustion is known to be significant, especially at take-off, where the maximum power of the engine is required. In the topic of combustion noise, the source mechanisms are usually separated between direct combustion noise, a monopolar source related to the pressure fluctuations generated by the turbulent flame in the combustion chamber, and indirect combustion noise, a dipolar source which

† Email address for correspondence: maxime.huet@onera.fr

https://doi.org/10.1017/jfm.2013.442 Published online by Cambridge University Press

corresponds to noise resulting from entropy or vorticity fluctuations being accelerated through a nozzle or a turbine stage.

Concerning indirect combustion noise, one can cite the early works of Candel (1972), Marble (1973) and Morfey (1973), amongst others, in the 1970s. Marble & Candel (1977) were among the first to quantify the noise generated by small-amplitude entropy spots convected through a compact nozzle, where the wavelengths are assumed to be large compared to the considered geometry. Cumpsty & Marble (1977) then extended this approach to entropy and vorticity spots passing through turbine rows. At the same time, Bohn (1977) demonstrated the importance of the nozzle shape on the generated noise for large frequencies and Bloy (1979) used the method of characteristics to calculate the pressure fluctuations generated by entropy spots of large amplitude passing through non-compact nozzles.

More recently, Stow, Dowling & Hynes (2002) and Goh & Morgans (2011) extended the compact solution of Marble & Candel (1977) to low frequencies using an effective nozzle length correction through an asymptotic expansion of the linearized Euler equations for supercritical nozzles. Moase, Brear & Manzie (2007), Giauque, Huet & Clero (2012) and Durán *et al.* generalized the approach of Marble and Candel to any non-compact nozzle by solving the linearized Euler equations in the frequency domain. It allowed them to compute the linear transfer functions for the upstream and downstream acoustic waves generated by an entropy forcing. The renewed interest in these analytical methods is especially motivated by the recent experimental results provided by the Deutsches Zentrum für Luft- und Raumfahrt (DLR) with the entropy wave generator (EWG) setup, where entropy spots of small amplitude are generated upstream of a flow accelerated through a nozzle. Experimental results have been analysed in detail by Bake *et al.* (2009). The acoustic levels were measured in the downstream section for variable operating conditions, varying from subsonic to supersonic diffusers with the presence of a shock. The shocked configuration was investigated numerically and analytically by Leyko *et al.* (2011) using large eddy simulation (LES) and Mühlbauer, Noll & Aigner (2009) with an unsteady Reynolds-averaged Navier–Stokes (URANS) approach. The subsonic configuration has been reproduced numerically by Mühlbauer *et al.* (2009), Giauque *et al.* (2012) and Durán, Moreau & Poinsot (2013*b*) and has also been investigated analytically by Howe (2010). Dealing with the turbine configuration, Leyko *et al.* (2010), Durán *et al.* (2013*a*) and Mishra & Bodony (2013) numerically investigated the actuator disk theory by comparing two-dimensional simulations with the analytical model of Cumpsty & Marble (1977) in the presence of small amplitude entropy perturbations. Leyko *et al.* and Durán *et al.* conducted LES of an isolated blade row and separate stator vane and rotor blade, respectively, while Mishra and Bodony performed Euler simulations of a flow past a realistic stator stage. They assessed the role of indirect combustion noise through a stator and a rotor and illustrated the limits of the compact model for perturbations with large frequencies.

With the exception of the study by Bloy (1979), all the above-mentioned works deal with small-amplitude perturbations and are related to linear regimes only. Although the linear approach is legitimate for mid- to high-frequency excitations which, having small wavelengths, are subject to intense turbulent dissipation in the burnt gas region before the nozzle or turbine stage, this approach might not always be adequate for low-frequency entropy excitations. At low frequency (typically below a few hundred Hz), the wavelength of such a fluctuation becomes comparable to the turbulent integral scale in the engine. Although obviously affected by the turbulent mixing cascade, no significant damping from the flame to the combustion chamber outlet is in

https://doi.org/10.1017/jfm.2013.442 Published online by Cambridge University Press

this case expected during the convection process. Recent studies have shown both numerically and experimentally the influence of coherent entropy waves on the onset or sustainability of combustion instabilities (Giauque 2007; Brear *et al.* 2012; Goh & Morgans 2013; Hochgreb *et al.* 2013; Motheau *et al.* 2013) and their role in acoustic mode scattering (Atassi & Gilson 2010). As such, it appears reasonable to consider the possibility that this kind of entropy perturbation also has amplitudes lying in the nonlinear domain (typically above 100 K for a 1000 K averaged background temperature). It is the objective of this work to study the indirect combustion noise generated by these low-frequency, nonlinear excitations. To do so, the analytical model of Marble and Candel for compact nozzles (Marble & Candel 1977), initially developed for excitations in the linear regime, is rederived and extended to the nonlinear domain.

The paper is organized as follows. In § 2, the fundamental equations for one-dimensional nonlinear acoustics are rederived in the presence of entropy perturbations. The analytical model is presented in § 3, where the full nonlinear and second-order Taylor expansion forms are given for both subcritical and supercritical configurations. Second-order analytical solutions are also provided. Section 4 deals with analyses of the second-order and full nonlinear solutions and, in particular, discusses the modifications of radiated noise with the amplitude of the excitation. The analytical solutions are then validated with comparisons to numerical simulations in § 5. Closing remarks are given in § 6.

2. Nonlinear acoustic equations

2.1. *Fundamental equations for an isentropic flow*

The derivation of the analytical model proposed by Marble & Candel (1977) requires the separation of the characteristic waves. By definition, the entropy wave is $\sigma = s'/c_p$ and, in the linear domain, the acoustic waves are given by $P^{\pm} = (p'/\gamma p_0 \pm u'/c_0)/2$, where s', p' and u' are the entropy, pressure and velocity perturbations, c_p and c_v are the heat capacity at constant pressure and volume, respectively, $\gamma = c_p/c_v$ is the adiabatic coefficient of the fluid and p_0 and c_0 are the pressure and sound velocity in the medium at rest. The entropy wave σ is convected by the flow and the acoustic waves P^+ and P^- propagate respectively in the downstream and upstream directions.

The acoustic wave decomposition mentioned above is valid in the linear domain but becomes inaccurate for high-amplitude perturbations, where a nonlinear expression of the characteristic waves is required. Such a nonlinear decomposition is derived here following the developments of Landau and Lifshitz for an isentropic gas flow (Landau & Lifshitz 1966). Let us first write the continuity and momentum equations for a one-dimensional inviscid flow:

$$\frac{\partial p}{\partial t} + u\frac{\partial p}{\partial x} + \rho c^2 \frac{\partial u}{\partial x} = 0, \tag{2.1}$$

$$\frac{\partial u}{\partial t} + u\frac{\partial u}{\partial x} + \frac{1}{\rho}\frac{\partial p}{\partial x} = 0, \tag{2.2}$$

where the density derivatives have been replaced by pressure derivatives in (2.1) using the formulas

$$\frac{\partial \rho}{\partial t} = \left(\frac{\partial \rho}{\partial p}\right)_s \frac{\partial p}{\partial t} = \frac{1}{c^2}\frac{\partial p}{\partial t}, \quad \frac{\partial \rho}{\partial x} = \frac{1}{c^2}\frac{\partial p}{\partial x}. \tag{2.3}$$

https://doi.org/10.1017/jfm.2013.442 Published online by Cambridge University Press

Dividing (2.1) by $\pm\rho c$ and adding it to (2.2), we obtain

$$\frac{\partial u}{\partial t} \pm \frac{1}{\rho c}\frac{\partial p}{\partial t} + (u \pm c)\left(\frac{\partial u}{\partial x} \pm \frac{1}{\rho c}\frac{\partial p}{\partial x}\right) = 0. \tag{2.4}$$

Let us now introduce the new unknown functions $J^{\pm} = u \pm \int \mathrm{d}p/\rho c$, which are called the Riemann invariants. The previous equation can be rewritten as

$$\left(\frac{\partial}{\partial t} + (u \pm c)\frac{\partial}{\partial x}\right) J^{\pm} = 0, \tag{2.5}$$

which indicates that the two quantities J^{+} and J^{-} are propagating with a constant amplitude with the phase velocities $u + c$ and $u - c$, respectively.

To evaluate the integral term $\int \mathrm{d}p/\rho c$ of $J^{\pm}$, we use the entropy differential for an ideal gas $\mathrm{d}s/c_p = \mathrm{d}T/T - (\gamma - 1)/\gamma \times \mathrm{d}p/p$, where T is the gas temperature, to write

$$\frac{\mathrm{d}p}{\rho c} = \frac{2}{\gamma - 1}\mathrm{d}c - \frac{c}{\gamma - 1}\frac{\mathrm{d}s}{c_p}. \tag{2.6}$$

In the case of an isentropic flow, $\mathrm{d}s = 0$ and (2.6) can be integrated analytically:

$$\int_{p_0}^{p} \frac{\mathrm{d}p}{\rho c} = \frac{2}{\gamma - 1}(c - c_0). \tag{2.7}$$

2.2. *Non-isentropic flow configuration*

In the presence of an entropy perturbation, (2.6) cannot be analytically integrated in the general case because $\mathrm{d}p/\rho c$ is no longer a perfect differential (Landau & Lifshitz 1966). More precisely, the integral $\int c\,\mathrm{d}s$ cannot be evaluated because the integrand is a function of the temperature and thus does not depend solely on the entropy variation but also on the pressure perturbation.

One may, however, evaluate this integral analytically by assuming a quasi-static evolution of the flow in the presence of the entropy fluctuation, that is, the flow goes through a sequence of states that are infinitesimally close to equilibrium. Under this hypothesis, the flow can be considered isentropic by using modified mean flow values that take into account the entropy fluctuation σ. In the present study, the entropy perturbations are assumed to be isobaric; the modified mean temperature and sound velocity are thus written as $T_0\mathrm{e}^{\sigma}$ and $c_0\mathrm{e}^{\sigma/2}$ respectively, where T_0 is the temperature in the medium at rest, and the Riemann invariants may be rewritten as

$$\Gamma^{\pm} = \frac{1}{2}\left(\frac{1}{c_0\mathrm{e}^{\sigma/2}}\int_{p_0}^{p}\frac{\mathrm{d}p}{\rho c} \pm \frac{u'}{c_0\mathrm{e}^{\sigma/2}}\right). \tag{2.8}$$

This form of the invariants is preferred to the expressions of $J^{\pm}$ because, for small-amplitude perturbations, it reduces to the expressions $P^{\pm}$ commonly used in the linear domain (Marble & Candel 1977; Leyko *et al.* 2011).

The quasi-static assumption thus allows analytical evaluation of the integral term $\int \mathrm{d}p/\rho c$ in the presence of an entropy perturbation. After some algebra, we find

$$\int_{p_0}^{p}\frac{\mathrm{d}p}{\rho c} = \frac{2}{\gamma - 1}\left(c - c_0\mathrm{e}^{\sigma/2}\right) = \frac{2c_0\mathrm{e}^{\sigma/2}}{\gamma - 1}\left(\left(1 + \frac{p'}{p_0}\right)^{(\gamma-1)/2\gamma} - 1\right). \tag{2.9}$$

https://doi.org/10.1017/jfm.2013.442 Published online by Cambridge University Press

One can now write explicitly the expression of the characteristic waves as functions of the flow perturbations,

$$\Gamma^{\pm} = \frac{1}{2}\left(\frac{2}{\gamma-1}\left(\left(1+\frac{p'}{p_0}\right)^{(\gamma-1)/2\gamma} - 1\right) \pm \frac{u'}{c_0 \mathrm{e}^{\sigma/2}}\right), \tag{2.10}$$

and, by considering the sum and the difference of the two waves and after some manipulations, express the flow perturbations as functions of the characteristic waves,

$$1+\frac{p'}{p_0} = \left(1+\frac{\gamma-1}{2}(\Gamma^{+}+\Gamma^{-})\right)^{2\gamma/(\gamma-1)}, \tag{2.11}$$

$$\frac{u'}{u_0} = \frac{1}{M_0 \mathrm{e}^{-\sigma/2}}(\Gamma^{+}-\Gamma^{-}), \tag{2.12}$$

where u_0 is the velocity in the medium at rest.

2.3. *Numerical validation*

The wave separation detailed above is now validated numerically by performing simulations in a one-dimensional channel. Simulations are performed with the code Sunday (SimUlation of Noise in 1D flows due to fluctuAtions in entropY) developed at ONERA (Giauque *et al.* 2012).

Sunday solves the quasi-one-dimensional nonlinear Euler equations for the primitive variables ρ, u and p. The full equations are first solved to provide the undisturbed steady flow. Then, perturbation equations are solved with either acoustic or entropy inlet disturbances, using nonlinear or linearized perturbation equations derived without the thermodynamically perfect gas assumption. The resolution is performed using finite differences. Space derivatives are computed using the optimized 11-point scheme and selective filter proposed by Bogey & Bailly (2004) and time integration is done with the standard explicit fourth-order Runge–Kutta algorithm. Centred schemes are used inside the computational domain and are switched to the upwind schemes proposed by Berland *et al.* (2007) near the boundaries. Centred and non-centred coefficients for the derivatives and the selective filtering can be found in de Cacqueray (2010).

Non-reflective boundary conditions are implemented at both extremities of the geometry using the characteristic boundary conditions proposed by Thompson (1987, 1990). In the present study, their numerical implementation follows the form given by Poinsot & Lele (1992). These conditions allow acoustic and entropy waves to leave the domain without noticeable reflections and are modified to inject pressure and temperature fluctuations (Kaufmann, Nicoud & Poinsot 2002). The reader may refer to Giauque *et al.* (2012) for additional details on the solver and its validation.

The gas used for the present simulation, performed in a duct of constant radius, is air with a constant heat capacity c_p. The mean flow has a temperature T_0 of 300 K, a pressure p_0 of 101 325 Pa and a velocity u_0 of 10 m s^{-1}. A uniform and steady entropy perturbation of amplitude $\sigma = s'/c_p = -0.5$ is superimposed on this flow.

The initial perturbed flow, represented in figure 1, is composed of two acoustic perturbations. Each perturbation has a Gaussian shape and is defined by the amplitude of its characteristic wave. The pulse Γ^{+} is centred on $x = -2$ m and propagates in the downstream direction whereas the pulse Γ^{-} is centred on $x = 3$ m and propagates in the upstream direction. Their amplitudes are chosen so that the maximum pressure perturbation corresponds to 20 and 15 % of the ambient pressure, respectively, which ensures a nonlinear propagation. The initial pressure and velocity perturbations

https://doi.org/10.1017/jfm.2013.442 Published online by Cambridge University Press

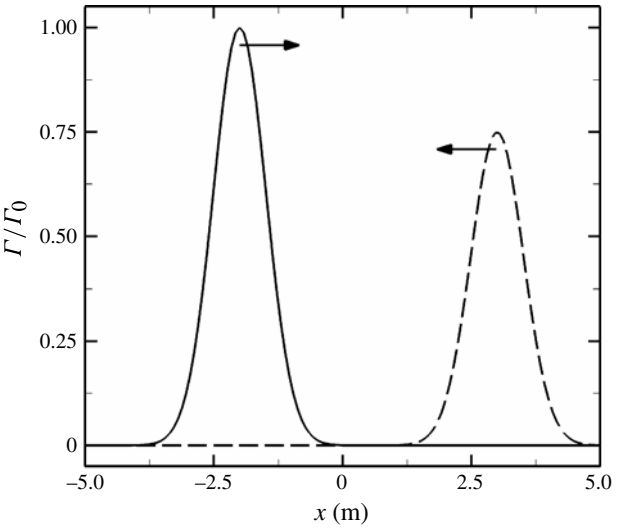


FIGURE 1. Amplitude of the two characteristic waves at $t = 0$: —, Γ^+, propagating in the $+x$ direction; - - -, Γ^-, propagating in the $-x$ direction.

are deduced from the characteristic waves using (2.11) and (2.12) and the initial temperature perturbation is obtained using the entropy relation in the perturbative form

$$\sigma = \ln \frac{1 + \dfrac{T'}{T_0}}{\left(1 + \dfrac{p'}{p_0}\right)^{(\gamma-1)/\gamma}}. \tag{2.13}$$

The flow variables are stored during the simulation at the position $x = 0$ and are used to separate the two characteristic waves using (2.10). Given the value of the acoustic Mach number $M_{ac} = u'_0/c_0$, where u'_0 is the amplitude of the acoustic velocity, the shock formation distance $l_s = \lambda/2\pi\beta M_{ac}$ (where λ is the acoustic wavelength and $\beta = (\gamma + 1)/2$) is large compared to the perturbation wavelength (Beyer 1997). Since this study focuses on nozzles that are compact with respect to the same perturbation wavelength, it is expected that the wave deformation will remain negligible through the nozzle. The time evolution of the two pulses is represented in figure 2 and is compared to the analytical solution obtained assuming that the two pulses do not interact with each other. One can see in this figure that the shapes and amplitudes of the simulated perturbations coincide very well with the analytical solution. The small time shift between the computed and theoretical signals, especially visible for the pulse Γ^-, comes from the interaction of the two pulses, which is not taken into account analytically; indeed, the pulse Γ^+ propagates with a positive velocity perturbation that decreases the propagation velocity of the pulse Γ^-.

These results validate the expressions of the characteristic waves in the nonlinear domain that are used in the present work and the capacity to separate those waves in the presence of an entropy perturbation using the quasi-static assumption. These simulations also illustrate the capability of the code Sunday to numerically reproduce nonlinear acoustic waves propagation in a non-isentropic flow.

https://doi.org/10.1017/jfm.2013.442 Published online by Cambridge University Press

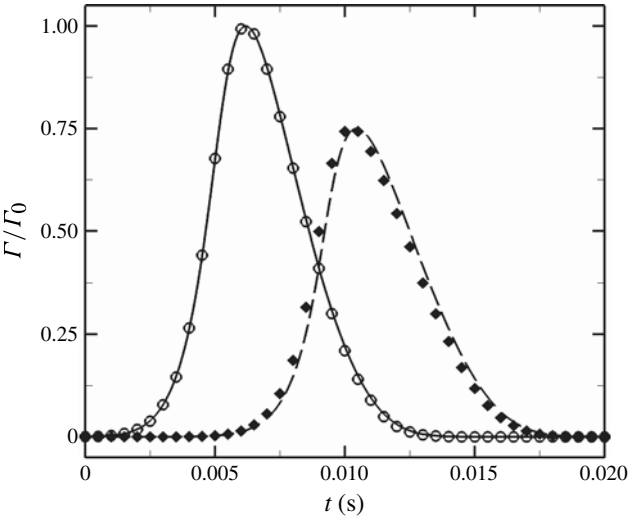


FIGURE 2. Time histories of the two characteristic waves at $x = 0$. Sunday: —, Γ^+; - - -, Γ^-. Analytical solution: ∘, Γ^+; ♦, Γ^-.

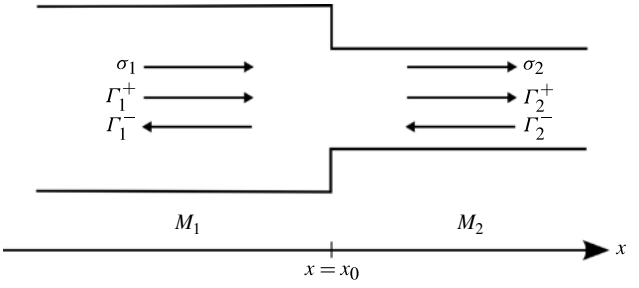


FIGURE 3. Sketch of the modelled compact nozzle with incoming and outcoming waves.

3. Analytical models

The amplitude of the acoustic waves generated upstream and downstream of a compact nozzle have been determined analytically in the linear domain by Marble and Candel for both acoustic and entropy forcings (Marble & Candel 1977). To this end, they consider a quasi-one-dimensional nozzle flow with adiabatic walls and a thermodynamically perfect gas, and assume that the nozzle is small with respect to the considered wavelengths so that it can be treated as a discontinuity. The flow itself inside the nozzle can thus be replaced by continuity relations for mass, stagnation temperature and entropy to evaluate the generated acoustic waves.

The model of Marble and Candel is rederived in this section and extended to the nonlinear regime with respect to the acoustic and entropy waves. Nonlinear analytical expressions of the generated waves are provided by writing second-order Taylor polynomials of the equations considered. An illustration of the compact nozzle used throughout the paper is reproduced in figure 3. The flow is oriented towards the increasing x-axis with the discontinuity located at $x = x_0$; $M = u/c$ stands for the Mach number, and upstream and downstream values are denoted by 1 and 2 respectively.

https://doi.org/10.1017/jfm.2013.442 Published online by Cambridge University Press

3.1. *Nonlinear model*

3.1.1. *Subcritical nozzle*

The flow is assumed to be isentropic and one-dimensional. A denotes the duct section. The flow is defined by its main characteristics such as its pressure p, density ρ and velocity u. Under these assumptions, the mass flow rate

$$\dot{m} = \rho u A, \tag{3.1}$$

the stagnation temperature

$$T_t = T\left(1 + \frac{\gamma - 1}{2} M^2\right), \tag{3.2}$$

and the entropy

$$s = c_p \ln \frac{p^{1/\gamma}}{\rho} \tag{3.3}$$

are constant upstream and downstream of the nozzle. By introducing the perturbed flow variables in the form $z_0\,(1 + z'/z_0)$, where z stands for any variable ρ, p, ..., and assuming an ideal gas, (3.1) and (3.2) can be expressed in perturbative form (see the Appendix). After some algebra and substitution of the natural variables with characteristics using (2.11)–(2.12), one obtains (3.4)–(3.6). For an acoustic forcing, (2.11)–(2.12) can be used without any hypothesis. In the case of an isobaric entropy excitation, relations (3.4)–(3.5) between the flow perturbations and the characteristics remain valid under the quasi-static flow hypothesis, so that

$$1 + \frac{\dot{m}'}{\dot{m}_0} = \left(1 + \frac{1}{M_0 \mathrm{e}^{-\sigma/2}}\left(\Gamma^+ - \Gamma^-\right)\right)\left(1 + \frac{\gamma - 1}{2}\left(\Gamma^+ + \Gamma^-\right)\right)^{2/(\gamma-1)} \mathrm{e}^{-\sigma}, \tag{3.4}$$

$$1 + \frac{T_t'}{T_{t0}} = \frac{1}{1 + \dfrac{\gamma - 1}{2} M_0^2}\left(\left(1 + \frac{\gamma - 1}{2}\left(\Gamma^+ + \Gamma^-\right)\right)^2 \mathrm{e}^{\sigma} + \frac{\gamma - 1}{2} M_0^2 \left(1 + \frac{1}{M_0 \mathrm{e}^{-\sigma/2}}\left(\Gamma^+ - \Gamma^-\right)\right)^2\right), \tag{3.5}$$

$$\frac{s'}{c_p} = \sigma. \tag{3.6}$$

Since the three quantities above are constant throughout the nozzle, the system to solve is written as

$$\left[\frac{\dot{m}'}{\dot{m}_0}\right]_1^2 = 0, \tag{3.7}$$

$$\left[\frac{T_t'}{T_{t0}}\right]_1^2 = 0, \tag{3.8}$$

$$\left[\frac{s'}{c_p}\right]_1^2 = 0, \tag{3.9}$$

where $[\ ]_1^2$ holds for the jump condition between the downstream (index 2) and upstream (index 1) parts of the nozzle.

3.1.2. *Supercritical nozzle*

The previous equations are valid for both subcritical and supercritical nozzles. A unique property of supercritical nozzles resides in the critical mass flow rate $\dot{m}_\star$, which

https://doi.org/10.1017/jfm.2013.442 Published online by Cambridge University Press

is imposed by the flow upstream of the nozzle throat and whose expression is given in the Appendix. Combining the critical mass flow rate fluctuation with the mass flow rate fluctuation used for the subcritical nozzle, one obtains after some algebra

$$0 = \left(1 + \frac{\gamma - 1}{2}\left(\Gamma^+ + \Gamma^-\right)\right)\left(1 + \frac{1}{M_0 \mathrm{e}^{-\sigma/2}}\left(\Gamma^+ - \Gamma^-\right)\right)^{-1} \mathrm{e}^{\sigma/2} \times \left[1 + \frac{\frac{\gamma - 1}{2}M_0^2}{1 + \frac{\gamma - 1}{2}M_0^2}\left(-1 + \left(1 + \frac{1}{M_0 \mathrm{e}^{-\sigma/2}}\left(\Gamma^+ - \Gamma^-\right)\right)^2 \times \left(1 + \frac{\gamma - 1}{2}\left(\Gamma^+ + \Gamma^-\right)\right)^{-2} \mathrm{e}^{-\sigma}\right)\right]^{(\gamma+1)/2(\gamma-1)} - 1. \tag{3.10}$$

This equation is rewritten for convenience as

$$F_\star = 0, \tag{3.11}$$

which holds both upstream and downstream of the nozzle, so that

$$[F_\star]_1 = 0, \tag{3.12}$$

$$[F_\star]_2 = 0, \tag{3.13}$$

where $[\ ]_i$ indicates that the expression is evaluated either in the upstream ($i = 1$) or downstream ($i = 2$) section.

3.2. *Second-order model*

The linear analytical solution provided by Marble & Candel (1977) is obtained by solving a first-order Taylor expansion of the equations above. The generated waves are written in the form $\Gamma^\pm/\varepsilon = \beta$, where ε is the excitation and β the solution of the system. For a harmonic excitation $\varepsilon = \varepsilon_0 \cos(\omega_0 t)$, the generated waves are also harmonic and at the same angular frequency ω_0. In this section, the Taylor expansion of the equations is extended to second order and solutions are sought in the form $\Gamma^\pm/\varepsilon = \alpha\varepsilon + \beta$, where α and β are real numbers. Considering the same harmonic forcing as above, the generated waves are now given by

$$\begin{aligned}\Gamma^\pm &= \alpha\varepsilon^2 + \beta\varepsilon \\ &= \tfrac{1}{2}\alpha\varepsilon_0^2 + \tfrac{1}{2}\alpha\varepsilon_0^2 \cos(2\omega_0 t) + \beta\varepsilon_0 \cos(\omega_0 t),\end{aligned} \tag{3.14}$$

which shows that the second-order solution does not modify the amplitude of the generated wave at the fundamental angular frequency ω_0 but predicts additional noise at the first harmonic $2\omega_0$. In the following, all mathematical expansions have been performed using the computer algebra system SAGE (Stein & Joyner 2005). The second-order Taylor expansions of (3.4) and (3.5) are respectively

$$\begin{aligned}\frac{\dot{m}'}{\dot{m}_0} = &\left(1 + \frac{1}{M_0}\right)\Gamma^+ + \left(1 - \frac{1}{M_0}\right)\Gamma^- - \sigma \\ &- \left(\frac{\gamma - 3}{4} - \frac{1}{M_0}\right)\Gamma^{+2} - \left(\frac{\gamma - 3}{4} + \frac{1}{M_0}\right)\Gamma^{-2} + \frac{1}{2}\sigma^2 \\ &- \frac{1}{2}(\gamma - 3)\,\Gamma^+\Gamma^- - \left(1 + \frac{1}{2M_0}\right)\Gamma^+\sigma - \left(1 - \frac{1}{2M_0}\right)\Gamma^-\sigma,\end{aligned} \tag{3.15}$$

https://doi.org/10.1017/jfm.2013.442 Published online by Cambridge University Press

$$\frac{T_t'}{T_{t0}} = \frac{1}{1+\dfrac{\gamma-1}{2}M_0^2}\left((\gamma-1)(1+M_0)\,\Gamma^+ + (\gamma-1)(1-M_0)\,\Gamma^- + \sigma \right.$$
$$+\frac{1}{4}(\gamma+1)(\gamma-1)\,\Gamma^{+2} + \frac{1}{4}(\gamma+1)(\gamma-1)\,\Gamma^{-2} + \frac{1}{2}\sigma^2$$
$$+\frac{1}{2}(\gamma-1)(\gamma-3)\,\Gamma^+\Gamma^- + (\gamma-1)\left(1+\frac{M_0}{2}\right)\Gamma^+\sigma$$
$$\left. +\,(\gamma-1)\left(1-\frac{M_0}{2}\right)\Gamma^-\sigma\right). \tag{3.16}$$

For the supercritical nozzle, (3.10) becomes

$$\left(1-\frac{\gamma-1}{2}M_0\right)\Gamma^+ - \left(1+\frac{\gamma-1}{2}M_0\right)\Gamma^- - \frac{1}{2}M_0\sigma$$
$$-\left(1-\frac{\gamma^2-1}{8}M+\frac{1}{M}-\frac{\gamma^2+2\gamma+1}{8(1+M)}\right.$$
$$\left.+\frac{\gamma^2-6\gamma+9}{8(1-M)}-\frac{(\gamma^2-6\gamma+9)M-4\gamma+12}{8\left(1+\dfrac{\gamma-1}{2}M^2\right)}\right)\Gamma^{+2}$$
$$+\left(1+\frac{\gamma^2-1}{8}M-\frac{1}{M}+\frac{\gamma^2-6\gamma+9}{8(1+M)}\right.$$
$$\left.-\frac{\gamma^2+2\gamma+1}{8(1-M)}+\frac{(\gamma^2-6\gamma+9)M+4\gamma-12}{8\left(1+\dfrac{\gamma-1}{2}M^2\right)}\right)\Gamma^{-2}$$
$$+\left(\frac{M}{4(\gamma-1)}+\frac{1}{8(1+M)}-\frac{1}{8(1-M)}+\frac{(\gamma-3)M}{8(\gamma-1)\left(1+\dfrac{\gamma-1}{2}M^2\right)}\right)\sigma^2$$
$$+\left(\frac{\gamma^2-1}{4}M+\frac{2}{M}+\frac{\gamma^2-2\gamma-3}{4(1+M)}-\frac{\gamma^2-2\gamma-3}{4(1-M)}+\frac{(\gamma^2-2\gamma-3)M}{4\left(1+\dfrac{\gamma-1}{2}M^2\right)}\right)\Gamma^+\Gamma^-$$
$$+\left(\frac{(\gamma-1)M+\gamma-3}{2(\gamma-1)}+\frac{\gamma+1}{4(1+M)}\right.$$
$$\left.-\frac{\gamma-3}{4(1-M)}+\frac{(\gamma^2-4\gamma+3)M-2\gamma+6}{4(\gamma-1)\left(1+\dfrac{\gamma-1}{2}M^2\right)}\right)\Gamma^+\sigma$$

https://doi.org/10.1017/jfm.2013.442 Published online by Cambridge University Press

$$+\left(\frac{(\gamma-1)M-\gamma+3}{2(\gamma-1)}+\frac{\gamma-3}{4(1+M)}\right.$$

$$\left.-\frac{\gamma+1}{4(1-M)}+\frac{(\gamma^2-4\gamma+3)M+2\gamma-6}{4(\gamma-1)\left(1+\dfrac{\gamma-1}{2}M^2\right)}\right)\Gamma^-\sigma$$

$$=0. \tag{3.17}$$

3.3. *Systems resolution*

For the subcritical nozzle, three waves may enter the domain, namely Γ_1^+, Γ_2^- and σ_1, and three waves must be determined, Γ_1^-, Γ_2^+ and σ_2: see figure 3. The amplitudes of the generated waves are obtained by solving (3.7)–(3.9) regardless of the types of the incoming waves entering the domain. In the supercritical case, the acoustic wave Γ_2^- represents an additional unknown. To complete the problem for that configuration, the mass flow equation (3.7) is replaced by (3.12) and (3.13). In practice, the full nonlinear system resolution is performed numerically using a Newton algorithm whereas an exact analytical solution can be expressed for the second-order system. For the sake of simplicity, the coupling between different excitations is not considered in the present paper: for any excitation Γ_1^+, Γ_2^- or σ_1, all other excitations are set to 0. This approach to the study of nonlinearities is legitimate because even thermo-acoustic instabilities can be analysed with success in the linear limit as far as acoustics is concerned (Paschereit *et al.* 2002; Boudier *et al.* 2009; Candel *et al.* 2012; Wolf *et al.* 2012). In this case, the study of superimposed acoustic and entropy excitations is straightforward because it corresponds to the summation of both linear and nonlinear responses.

The resolution of the nonlinear systems provides the amplitude of the generated waves $\Gamma^\pm$ with respect to the amplitude of the excitation ε. To investigate the influence of the forcing amplitude on the wave generation, it is convenient to use the extended nozzle describing functions that represent the non-dimensional generated waves $\Gamma^\pm/\varepsilon$ as functions of the forcing ε. This representation extends the usual describing function (Noiray *et al.* 2008) by providing the full nonlinear response of the system. A linear evolution of the extended describing functions is sought for the second-order system resolution, that is, the wave amplitudes are given by $\Gamma^\pm/\varepsilon = \alpha\varepsilon + \beta$, where β is the linear nozzle response of Marble & Candel (1977) and α is the slope of the nozzle response with respect to the forcing amplitude when $\varepsilon \to 0$. The resolution procedure for the second-order system is detailed in the case of a supercritical nozzle flow excited by an entropy disturbance. The successive steps of the resolution are summarized in figure 4. A similar resolution may be applied to an acoustic forcing and in the subsonic case. The resolution is based on successive substitutions and Taylor expansions of the generated characteristic wave expressions into the conservation equations.

Step 1. Equation (3.9) indicates that the entropy fluctuation is conserved through the nozzle. Upstream and downstream entropy waves can therefore be simplified in the polynomial system $\sigma_1 = \sigma_2 = \sigma$.

Step 2. Using (3.12), one can express the wave Γ_1^- as a function of the forcing σ and flow characteristics only. Since equation (3.12) is a second-order polynomial, two solutions are available for Γ_1^-. One can discriminate between the physical and non-physical solutions because the non-physical solution has a non-zero amplitude

https://doi.org/10.1017/jfm.2013.442 Published online by Cambridge University Press

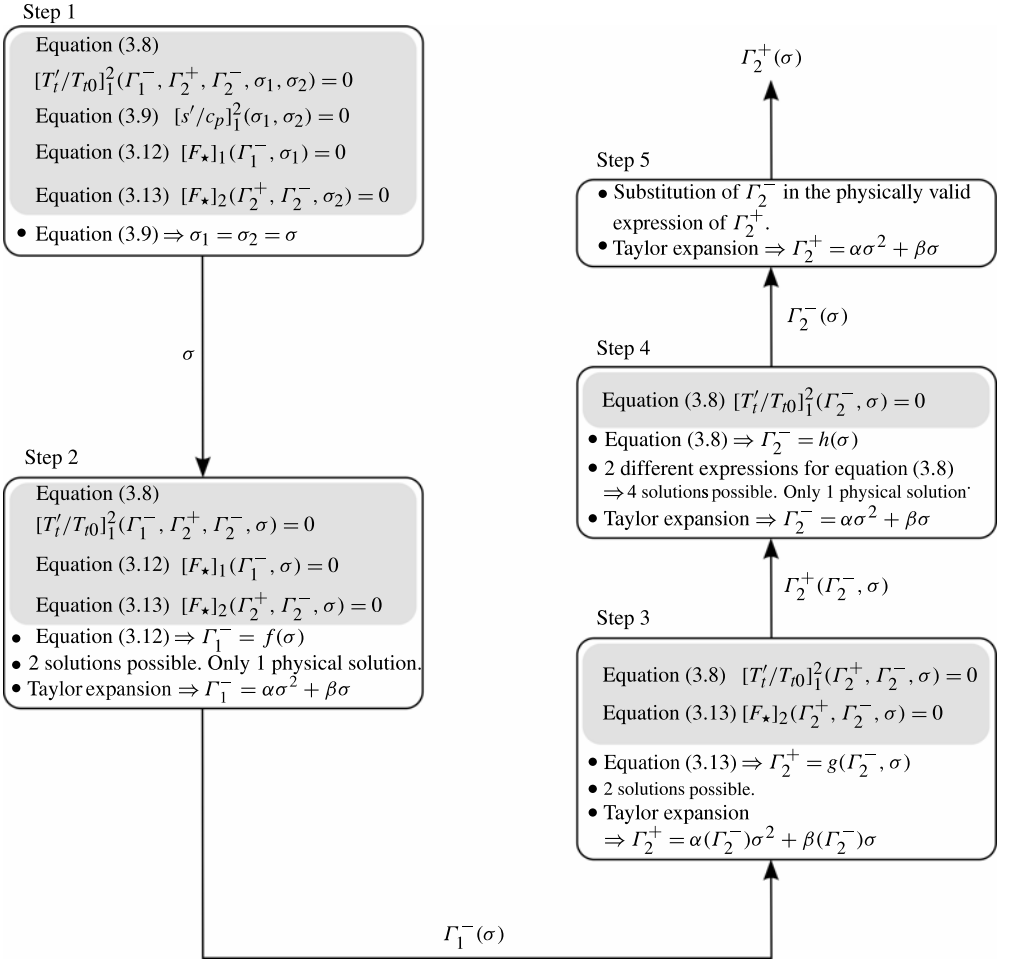


FIGURE 4. Summary of the resolution steps for the second-order system for a supercritical nozzle flow with entropy forcing.

even in the absence of excitation. The linear evolution of Γ_1^-/σ with respect to the forcing σ is then obtained using a Taylor expansion of the physical solution with respect to σ, after which Γ_1^- is replaced by substituting its solution into (3.8) and (3.13).

Step 3. Equation (3.13) is now used to express Γ_2^+ with respect to Γ_2^- and σ. The two solutions are developed in polynomials with a second-order Taylor expansion with respect to Γ_2^- and σ and substituted into (3.8).

Step 4. The previous substitution leads to two different expressions of the stagnation temperature conservation, further simplified into second-order polynomials and depending only on Γ_2^- and σ. The resolution of these two equations finally provides four different expressions for Γ_2^-/σ, three of them diverging for $\sigma \to 0$ and therefore being non-physical.

Step 5. To finish, the Taylor expansion of the physical solution for Γ_2^- is used to write Γ_2^+ as a function of σ only, this wave solution being expressed as a second-order polynomial with respect to σ thanks to a Taylor expansion.

https://doi.org/10.1017/jfm.2013.442 Published online by Cambridge University Press

$$\Gamma_1^- \quad \alpha = -\frac{M_1}{(1-M_1)^3}\frac{1}{1+M_2}\frac{M_2-M_1}{(M_2+M_1)^2}\frac{\left(1+\frac{1}{2}(\gamma-1)M_1^2\right)\left(1+\frac{1}{2}(\gamma-1)M_2^2\right)}{\left(1+\frac{1}{2}(\gamma-1)M_1M_2\right)^3}$$

$$\times\left[(\gamma-1)M_1^2M_2^3+(\gamma-1)M_1^2M_2^2-(\gamma-3)M_1^2M_2-(\gamma-3)M_2^2-2M_2-2\right]$$

$$\beta = \left(\frac{M_2-M_1}{1-M_1}\right)\left(\frac{1+M_1}{M_2+M_1}\right)\left[\frac{1-\frac{1}{2}(\gamma-1)M_1M_2}{1+\frac{1}{2}(\gamma-1)M_1M_2}\right]$$

$$\Gamma_2^+ \quad \alpha = -\frac{M_2}{(1+M_2)^3}\frac{1}{1-M_1}\frac{M_2-M_1}{(M_2+M_1)^2}\frac{\left(1+\frac{1}{2}(\gamma-1)M_2^2\right)\left(1-\frac{1}{2}(\gamma-1)M_2\right)^2}{\left(1+\frac{1}{2}(\gamma-1)M_1M_2\right)^3}$$

$$\times\left[(\gamma-1)M_1^3M_2^2-(\gamma-1)M_1^2M_2^2-(\gamma-3)M_1M_2^2+(\gamma-3)M_1^2-2M_1+2\right]$$

$$\beta = \left(\frac{2M_2}{1+M_2}\right)\left(\frac{1+M_1}{M_2+M_1}\right)\left[\frac{1+\frac{1}{2}(\gamma-1)M_2^2}{1+\frac{1}{2}(\gamma-1)M_1M_2}\right]$$

TABLE 1. Second-order analytical solutions for the subcritical nozzle with upstream acoustic wave forcing Γ_1^+. Solutions of the form $\Gamma^\pm/\Gamma_1^+ = \alpha\Gamma_1^+ + \beta$.

The coefficients α and β of the second-order analytical solutions are reproduced in tables 1–3 for the subcritical nozzle and in table 4 for the supercritical nozzle. For both configurations, it has been verified that the linear nozzle response of Marble & Candel (1977) is recovered through the coefficient β. One also observes for the supercritical nozzle with acoustic forcing that $\alpha = 0$. It has been verified analytically that the first-order solution is indeed the exact solution of the full nonlinear equations, indicating that nonlinear effects do not modify the supercritical nozzle response to incoming acoustic waves.

4. Detailed investigation of the extended nozzle describing functions

In the previous section, the extended nozzle describing functions were provided for both acoustic and entropy forcings. In practical applications, nonlinear acoustic fluctuations are rarely observed because they correspond to very high pressure fluctuations that are seldom generated even in the case of combustion instabilities (Paschereit *et al.* 2002; Boudier *et al.* 2009; Candel *et al.* 2012; Wolf *et al.* 2012). However, recent studies have evidenced the role of coherent entropy waves in the onset or sustainability of combustion instabilities (Giauque 2007; Brear *et al.* 2012; Motheau *et al.* 2013) and it appears reasonable to consider the possibility that this kind of perturbation also has amplitudes lying in the nonlinear domain. The rest of the paper therefore focuses on detailed analyses corresponding to entropy forcings.

https://doi.org/10.1017/jfm.2013.442 Published online by Cambridge University Press

$$\Gamma_1^- \quad \alpha = -\frac{M_1}{(1-M_1)^3}\frac{1}{1+M_2}\frac{M_2-M_1}{(M_2+M_1)^2}\frac{\left(1+\frac{1}{2}(\gamma-1)M_1^2\right)\left(1+\frac{1}{2}(\gamma-1)M_1\right)^2}{\left(1+\frac{1}{2}(\gamma-1)M_1M_2\right)^3}$$

$$\times\left[(\gamma-1)M_1^2M_2^3+(\gamma-1)M_1^2M_2^2-(\gamma-3)M_1^2M_2-(\gamma-3)M_2^2-2M_2-2\right]$$

$$\beta = \left(\frac{2M_1}{M_1+M_2}\right)\left(\frac{1-M_2}{1-M_1}\right)\left[\frac{1+\frac{1}{2}(\gamma-1)M_1^2}{1+\frac{1}{2}(\gamma-1)M_1M_2}\right]$$

$$\Gamma_2^+ \quad \alpha = -\frac{M_2}{(1+M_2)^3}\frac{1}{1-M_1}\frac{M_2-M_1}{(M_2+M_1)^2}\frac{\left(1+\frac{1}{2}(\gamma-1)M_1\right)^2\left(1+\frac{1}{2}(\gamma-1)M_2^2\right)}{\left(1+\frac{1}{2}(\gamma-1)M_1M_2\right)^3}$$

$$\times\left[(\gamma-1)M_1^3M_2^2-(\gamma-1)M_1^2M_2^2-(\gamma-3)M_1M_2^2+(\gamma-3)M_1^2-2M_1+2\right]$$

$$\beta = -\left(\frac{M_2-M_1}{1+M_2}\right)\left(\frac{1-M_2}{M_2+M_1}\right)\left[\frac{1-\frac{1}{2}(\gamma-1)M_1M_2}{1+\frac{1}{2}(\gamma-1)M_1M_2}\right]$$

TABLE 2. Second-order analytical solutions for the subcritical nozzle with downstream acoustic wave forcing Γ_2^-. Solutions of the form $\Gamma^\pm/\Gamma_2^- = \alpha\Gamma_2^- + \beta$.

4.1. *Restriction of the excitation amplitude for nozzle flow regime conservation*

The entropy excitation is related to a temperature fluctuation that modifies the local sound velocity. Moreover, the generated acoustic waves propagate upstream and downstream of the nozzle with velocity and temperature fluctuations. All these flow perturbations lead to modification of the local Mach number. The analytical approach developed in § 3 remains valid only if the flow regime does not change through time while the temperature perturbation goes through the nozzle, i.e. the flow does not switch from subsonic to supersonic or vice versa. This imposes a constraint on the amplitude of the entropy forcing considered that can be determined numerically.

The mean Mach number is given by $M_0 = u_0/c_0$ and is modified to $M = (u_0+u')/(c_0\sqrt{1+T'/T_0})$ in the presence of perturbations. Using (2.11)–(2.13), the fluctuating Mach number can be rewritten as a function of the mean Mach number and the characteristic waves:

$$M_0 + M' = \frac{M_0 e^{-\sigma/2} + \left(\Gamma^+ - \Gamma^-\right)}{1+\frac{1}{2}(\gamma-1)\left(\Gamma^+ + \Gamma^-\right)}. \tag{4.1}$$

The flow regime is not modified as long as $0 < M_0 + M' < 1$ in the subsonic regime and $M_0 + M' > 1$ in the supersonic regime.

Figure 5 illustrates the maximum harmonic entropy forcing amplitude that can be applied without flow regime modification, with respect to upstream and downstream mean Mach numbers. Restrictions are visible for subcritical nozzles with significant

https://doi.org/10.1017/jfm.2013.442 Published online by Cambridge University Press

$$\Gamma_1^- \quad \alpha = -\frac{1}{32}\frac{M_1}{(1-M_1)^3}\frac{M_2-M_1}{1+M_2}\frac{1}{\left(1+\frac{1}{2}(\gamma-1)M_1M_2\right)^3}$$
$$\times\left[2\left(\gamma^2-2\gamma+1\right)M_1^3M_2^3-\left(\gamma^2-4\gamma+3\right)M_1^4M_2+2\left(\gamma^2-4\gamma+3\right)M_1^3M_2^2\right.$$
$$-\left(\gamma^2-4\gamma+3\right)M_1^2M_2^3-4(\gamma-1)M_1^3M_2-2\left(\gamma^2-8\gamma+7\right)M_1^2M_2^2$$
$$+4(\gamma-1)M_1^2M_2-4(\gamma-1)M_1M_2^2-2(\gamma+1)M_1^2$$
$$\left.-4(\gamma-3)M_1M_2-2(\gamma-3)M_2^2+8M_1-8M_2-8\right]$$
$$\beta = -\left(\frac{M_2-M_1}{1-M_1}\right)\frac{\frac{1}{2}M_1}{1+\frac{1}{2}(\gamma-1)M_1M_2}$$

$$\Gamma_2^+ \quad \alpha = \frac{1}{32}\frac{M_2}{(1+M_2)^3}\frac{M_2-M_1}{1-M_1}\frac{1}{\left(1+\frac{1}{2}(\gamma-1)M_1M_2\right)^3}$$
$$\times\left[2\left(\gamma^2-2\gamma+1\right)M_1^3M_2^3+\left(\gamma^2-4\gamma+3\right)M_1^3M_2^2-2\left(\gamma^2-4\gamma+3\right)M_1^2M_2^3\right.$$
$$+\left(\gamma^2-4\gamma+3\right)M_1M_2^4-2\left(\gamma^2-8\gamma+7\right)M_1^2M_2^2-4(\gamma-1)M_1M_2^3$$
$$+4(\gamma-1)M_1^2M_2-4(\gamma-1)M_1M_2^2-2(\gamma-3)M_1^2$$
$$\left.-4(\gamma-3)M_1M_2-2(\gamma+1)M_2^2+8M_1-8M_2-8\right]$$
$$\beta = \left(\frac{M_2-M_1}{1+M_2}\right)\frac{\frac{1}{2}M_2}{1+\frac{1}{2}(\gamma-1)M_1M_2}$$

TABLE 3. Second-order analytical solutions for the subcritical nozzle with entropy forcing σ. Solutions of the form $\Gamma^{\pm}/\sigma = \alpha\sigma + \beta$.

inlet or outlet Mach numbers, where the flow transition is observed even for very low-amplitude entropy excitations.

These restrictions on the maximum forcing amplitude can be interpreted physically assuming linear perturbations. As mentioned above, the flow regime modification is related to the evolution of the ratio $(1+u'/u_0)/\sqrt{1+T'/T_0}$. In the subcritical regime, for instance, the transition to supersonic occurs if $M' > 0$, which corresponds to $(1+u'/u_0)/\sqrt{1+T'/T_0} > 1$. Linearization of (2.11)–(2.13) permits us to express velocity and temperature perturbations as functions of the characteristics for small-amplitude perturbations,

$$u'/u_0 = \frac{1}{M_0}(\Gamma^+ - \Gamma^-), \tag{4.2}$$

$$\sqrt{1+T'/T_0} = 1 + \frac{1}{2}\left(\sigma + (\gamma-1)(\Gamma^+ + \Gamma^-)\right), \tag{4.3}$$

https://doi.org/10.1017/jfm.2013.442 Published online by Cambridge University Press

	Upstream acoustic wave forcing ($\varepsilon = \Gamma_1^+$)	Entropy wave forcing ($\varepsilon = \sigma$)
Γ_1^-	$\alpha = 0$	$\alpha = \dfrac{\frac{1}{8}M_1}{1+\frac{1}{2}(\gamma-1)M_1}$
	$\beta = \dfrac{1-\frac{1}{2}(\gamma-1)M_1}{1+\frac{1}{2}(\gamma-1)M_1}$	$\beta = -\dfrac{\frac{1}{2}M_1}{1+\frac{1}{2}(\gamma-1)M_1}$
Γ_2^+	$\alpha = 0$	$\alpha = -\dfrac{M_2-M_1}{2}\dfrac{\frac{1}{8}}{1+\frac{1}{2}(\gamma-1)M_1}$
	$\beta = \dfrac{1+\frac{1}{2}(\gamma-1)M_2}{1+\frac{1}{2}(\gamma-1)M_1}$	$\beta = \left(\dfrac{M_2-M_1}{2}\right)\dfrac{\frac{1}{2}}{1+\frac{1}{2}(\gamma-1)M_1}$
Γ_2^-	$\alpha = 0$	$\alpha = \dfrac{M_2+M_1}{2}\dfrac{\frac{1}{8}}{1+\frac{1}{2}(\gamma-1)M_1}$
	$\beta = \dfrac{1-\frac{1}{2}(\gamma-1)M_2}{1+\frac{1}{2}(\gamma-1)M_1}$	$\beta = -\left(\dfrac{M_2+M_1}{2}\right)\dfrac{\frac{1}{2}}{1+\frac{1}{2}(\gamma-1)M_1}$

TABLE 4. Second-order analytical solutions for the supercritical nozzle. Solutions of the form $\Gamma^\pm/\varepsilon = \alpha\varepsilon + \beta$.

with $\Gamma^\pm = \beta\sigma$. The latter equation exhibits both contributions of entropy and acoustics to the temperature fluctuation. For a diatomic gas, $\beta > -0.5$ for all subsonic configurations (see figure 11, studied in detail in § 4.3); temperature fluctuations are therefore of the same sign as entropy fluctuations.

Let us first investigate the Mach number fluctuations in the subsonic regime. Upstream of the nozzle, $\Gamma_1^+ = 0$ and the velocity fluctuation is given by $u_1'/u_1 = -\beta\sigma/M_1$, with $\beta \to +\infty$ when $M_1 \to 1$. For a negative entropy forcing, large positive velocity fluctuations occur while the temperature is decreased, leading to an increase of the Mach number that primes the nozzle. In the low Mach number limit, $M_1 \to 0$, the velocity perturbation is given by $u_1'/u_1 = M_2\sigma$ and therefore remains negligible compared to the flow mean velocity. It ensures that the Mach number remains positive regardless of the forcing amplitude.

In the downstream region, $\Gamma_2^- = 0$ and the velocity fluctuation is given by $u_2'/u_2 = \beta\sigma/M_2$, with $\beta > 0$ when $M_2 \to 1$. Velocity and temperature perturbations are therefore of the same sign and one cannot tell whether the Mach number increases or decreases with their fluctuation. To evaluate more precisely the Mach number variation,

https://doi.org/10.1017/jfm.2013.442 Published online by Cambridge University Press

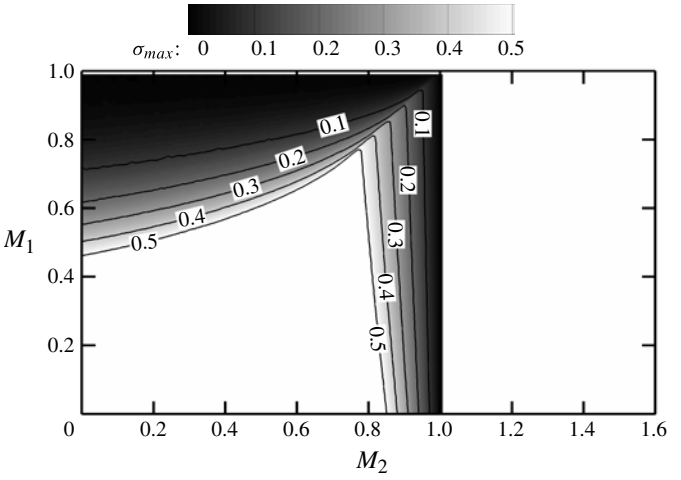


FIGURE 5. Maximum entropy forcing σ_{max} that can be applied without flow regime modification, with respect to subsonic upstream (M_1) and arbitrary downstream (M_2) Mach numbers for a diatomic gas ($\gamma = 1.4$).

we linearize (4.1) on the perturbed Mach number

$$M' = -\frac{1}{2}M_0\sigma + \left(1 - \frac{\gamma-1}{2}M_0\right)\Gamma^+ - \left(1 + \frac{\gamma-1}{2}M_0\right)\Gamma^-, \tag{4.4}$$

which is written as $M_2' = -\sigma/2 + (1-(\gamma-1)/2)\,\Gamma_2^+$ downstream of a subcritical nozzle when $M_2 \to 1$. The linear response is given by $\Gamma_2^+ = \beta\sigma$ and the previous equation can be factorized as $M_2' = \chi\sigma$. A specific investigation shows that $\chi > 0$, so that the perturbed Mach number is increased and the regime switches to supersonic for positive entropy forcings. As for the upstream region, in the low Mach number limit the velocity perturbation is given by $u_2'/u_2 = M_1\sigma$ downstream of the nozzle. There is thus no restriction on the forcing amplitude when $M_2 \to 0$.

Using the same method, one shows that there are no upstream and downstream Mach number fluctuations in the supersonic regime. The linear approach therefore predicts no limitation in the maximum entropy forcing amplitude. It has been verified numerically that this particular behaviour of supercritical nozzles remains valid even for nonlinear forcing amplitudes.

4.2. *Accuracy of the second-order model*

The accuracy of the second-order model is evaluated by comparing the predicted extended nozzle describing functions with those provided by the full nonlinear model, for the maximum possible harmonic entropy forcings σ_{max} keeping the flow regimes unchanged. For the cases where the maximum forcing is very large, its value is capped at $\sigma_{max} = 0.5$, a value thought to overestimate the maximum physical entropy fluctuation that can occur in real combustion chambers.

The difference between the second-order model and the full nonlinear analytic solutions is reproduced in figure 6 for any subsonic upstream Mach number M_1 and both subsonic and supersonic downstream Mach numbers M_2 without shock. This difference is expressed as the maximum relative error between the second-order and full nonlinear solutions for all excitation amplitudes $|\sigma| \leqslant \sigma_{max}$:

https://doi.org/10.1017/jfm.2013.442 Published online by Cambridge University Press

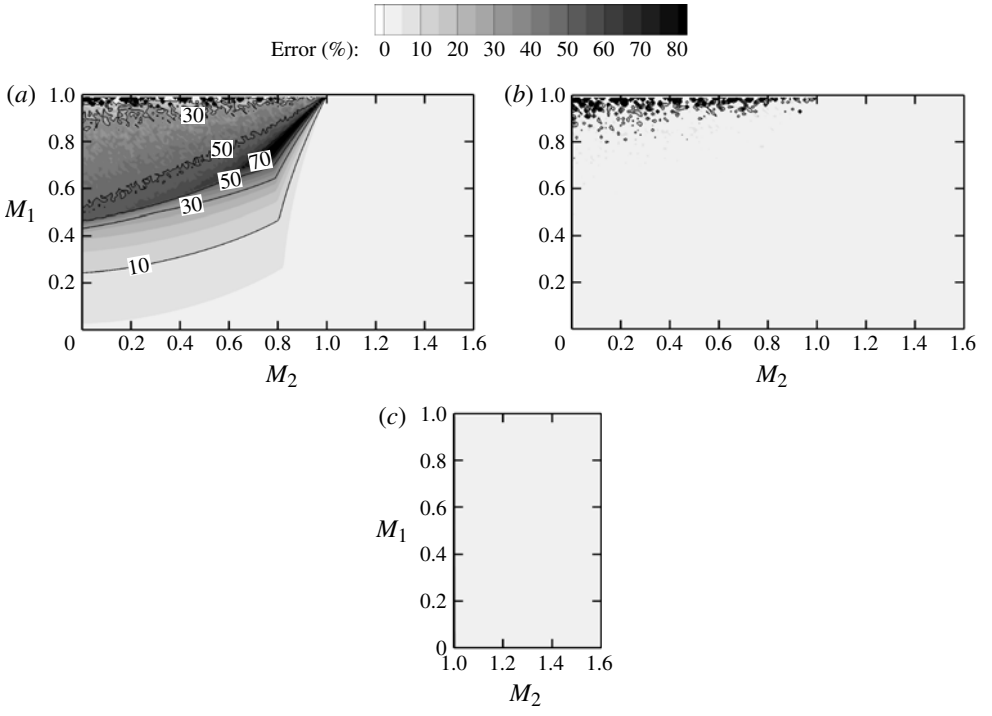


FIGURE 6. Maximum relative error of the second-order model with comparison to the full nonlinear nozzle response for a harmonic entropy forcing with $\sigma_{max} \leqslant 0.5$. Diatomic gas, $\gamma = 1.4$: (*a*) Γ_1^-/σ; (*b*) Γ_2^+/σ; (*c*) Γ_2^-/σ.

$|(\Gamma_{order\ 2} - \Gamma_{nonlinear})/\Gamma_{nonlinear}|$. One first observes in this figure that the second-order model is very accurate in the supercritical regime regardless of the type of wave considered, the error being of 1 %. In the subcritical regime, the error is negligible for Γ_2^+ for all Mach numbers and remains low for Γ_1^- for almost all converging geometries. For those configurations, the flow nonlinearities therefore lead essentially to the generation of additional noise at the first harmonic of the forcing frequency. The error is more important for Γ_1^- for diverging nozzles, especially for high subsonic values of M_1 and M_2 where the discrepancy between second-order and full nonlinear solutions may rise above 70 %. For these geometries, contributions of high-order nonlinearities (perturbations of order 3 and above) become important and lead to strong modifications of the generated acoustic wave Γ_1^- compared to the linear regime. It is important to note that, in the regime of most relevance for turbine combustors where M_1 is small and M_2 is significant, the second-order model is very accurate.

The extended nozzle describing functions of a subcritical converging nozzle ($M_1 = 0.1$, $M_2 = 0.3$) are represented in figure 7. The non-dimensionalized pressure fluctuations computed by both second-order and full nonlinear models are plotted with respect to the forcing amplitude σ. They correspond to the acoustic perturbations generated when an entropy spot of amplitude σ is accelerated through the nozzle. For this configuration, the fluctuations computed using both models are in good agreement, with a level difference below 6 % for both waves Γ_1^- and Γ_2^+. It means that the acceleration of an entropy spot with a large amplitude will not modify the non-dimensionalized amplitude of the acoustic wave at the fundamental frequency of the

https://doi.org/10.1017/jfm.2013.442 Published online by Cambridge University Press

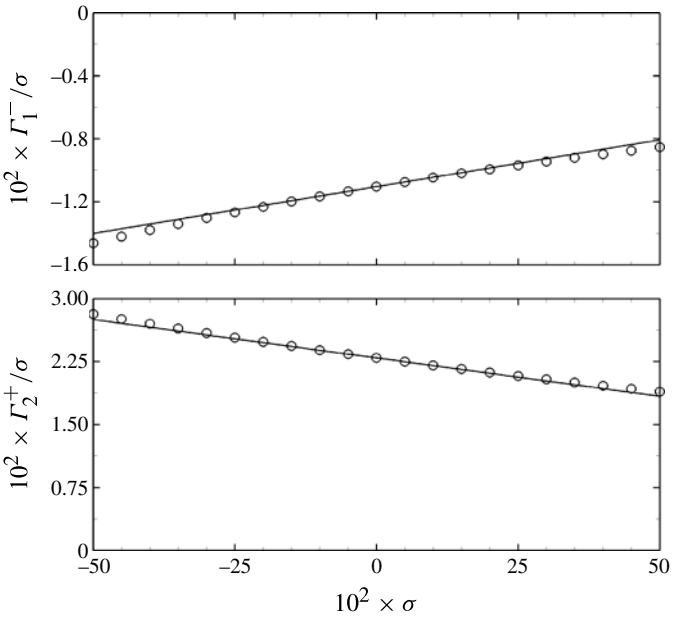


FIGURE 7. Extended nozzle describing functions of a subcritical converging nozzle with $M_1 = 0.1$, $M_2 = 0.3$ and $\gamma = 1.4$: ∘, full nonlinear solution; —, second-order solution.

forcing, but will lead to the generation of additional noise at the first harmonic of the forcing frequency solely.

To illustrate the discrepancies that may occur between the second-order and full nonlinear solutions, the extended nozzle describing functions of a subcritical diverging nozzle for $M_1 = 0.5$ and $M_2 = 0.2$ are considered in figure 8. For this regime, the error remains negligible for the downstream wave Γ_2^+ but is more visible for the upstream wave Γ_1^-. The second-order solution slowly departs from the full nonlinear evolution for positive forcings with a maximum underestimation of 35 % for $\sigma = 0.5$. The discrepancy is even more obvious for negative forcings, where both solutions start to mismatch strongly for $\sigma < -0.3$ with a large increase of the full nonlinear solution and a relative error of the second-order model of -45 % for $\sigma = -0.5$. The generation of a rich acoustic spectrum, with several harmonics, can thus be expected for Γ_1^- for this configuration.

Figure 9 illustrates the power spectral densities of the wave Γ_1^-, computed using the full nonlinear solution and generated by harmonic entropy forcings of varying amplitude, for the two nozzle regimes presented above. The left figure corresponds to the converging nozzle of figure 7, where full nonlinear and second-order models collapse. As expected theoretically, increasing the forcing amplitude does not modify the amplitude of the fundamental frequency but essentially generates additional noise for the first harmonic of the forcing, with an amplitude at least 17 dB below that of the fundamental frequency (amplitude ratio of 7). The extra noise observed for larger frequencies is a consequence of the small discrepancies observed between the second and full nonlinear solutions. The contribution of these harmonics is nevertheless several decades lower than that of the first two frequencies and can therefore be neglected. The time signatures of the wave Γ_1^-/σ_0 for the different amplitudes of the entropy forcing σ_0 are plotted in figure 10(*a*). This figure especially exhibits the

https://doi.org/10.1017/jfm.2013.442 Published online by Cambridge University Press

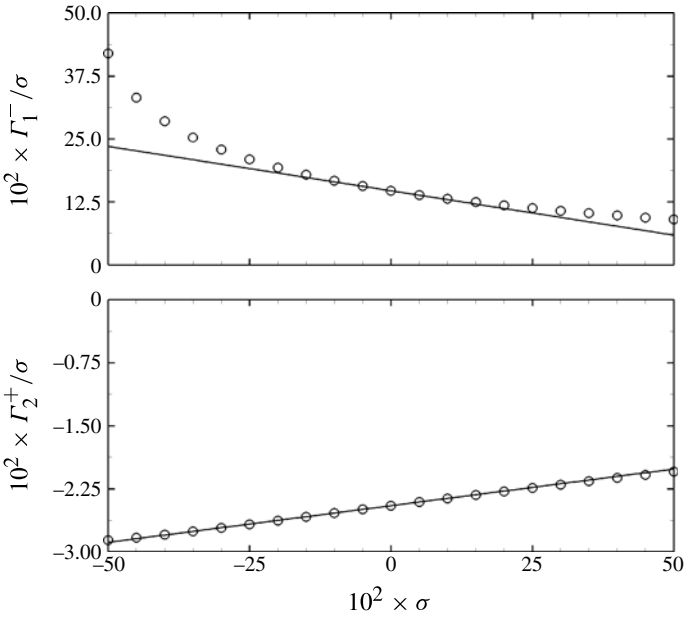


FIGURE 8. Extended nozzle describing functions of a subcritical diverging nozzle with $M_1 = 0.5$, $M_2 = 0.2$ and $\gamma = 1.4$: ∘, full nonlinear solution; —, second-order solution.

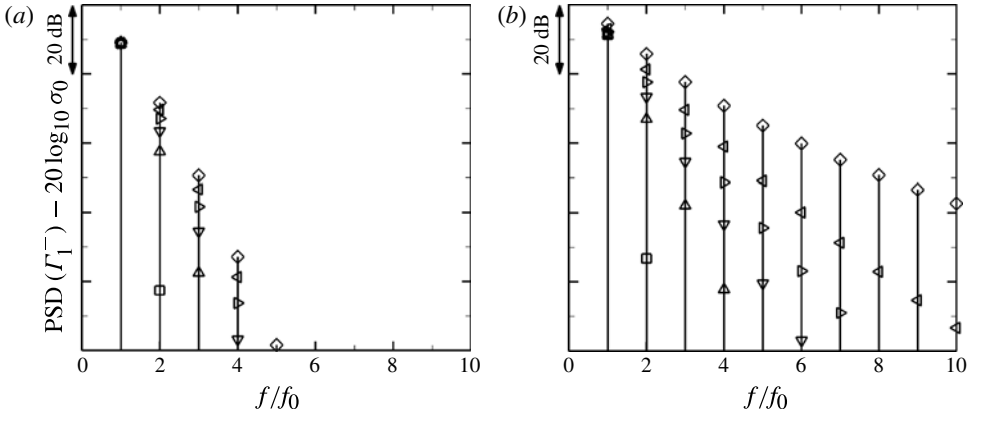


FIGURE 9. Non-dimensionalized power spectral density of the wave Γ_1^- generated by a harmonic entropy forcing of amplitude σ_0 and frequency f_0 for different nozzle geometries and entropy forcing amplitudes: □, $\sigma_0 = 10^{-3}$; △, $\sigma_0 = 0.1$; ▽, $\sigma_0 = 0.2$; ▷, $\sigma_0 = 0.3$; ◁, $\sigma_0 = 0.4$; ◇, $\sigma_0 = 0.5$. Diatomic gas simulations ($\gamma = 1.4$) with the full nonlinear model: (*a*) subcritical converging nozzle, $M_1 = 0.1, M_2 = 0.3$; (*b*) subcritical diverging nozzle, $M_1 = 0.5, M_2 = 0.2$.

modification of the signal shape with the increasing amplitude of the forcing, coming from the rising level of the first harmonic of the acoustic signal.

The power spectral densities of the wave Γ_1^- calculated with the full nonlinear model are displayed in figure 9(*b*) for the diverging geometry, where second-order and full nonlinear solutions significantly differ. The highly nonlinear evolution of

https://doi.org/10.1017/jfm.2013.442 Published online by Cambridge University Press

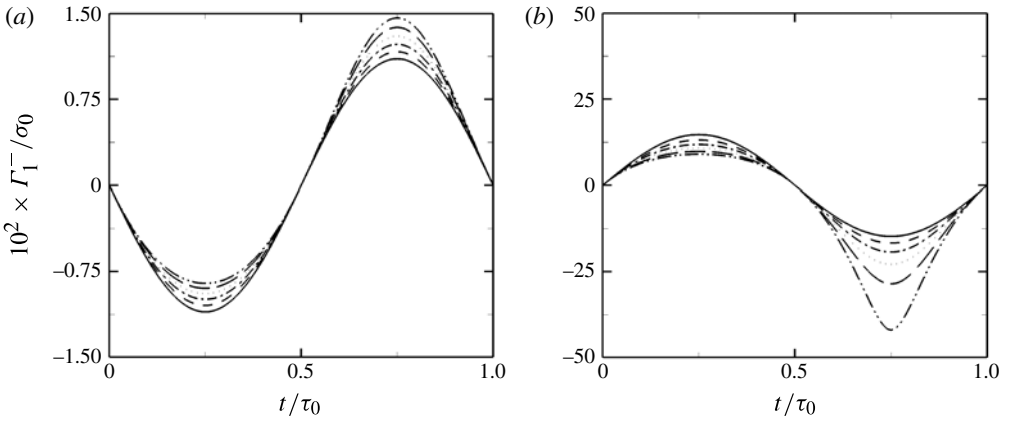


FIGURE 10. Time signature of the wave Γ_1^- generated by a harmonic entropy forcing $\sigma = \sigma_0 \sin(2\pi t/\tau_0)$ for different nozzle geometries and entropy forcing amplitudes: —, $\sigma_0 = 10^{-3}$; – – –, $\sigma_0 = 0.1$; – · –, $\sigma_0 = 0.2$; · · ·, $\sigma_0 = 0.3$; — —, $\sigma_0 = 0.4$; — · ·, $\sigma_0 = 0.5$. Diatomic gas simulations ($\gamma = 1.4$) with the full nonlinear model: (*a*) subcritical converging nozzle, $M_1 = 0.1, M_2 = 0.3$; (*b*) subcritical diverging nozzle, $M_1 = 0.5, M_2 = 0.2$.

the extended nozzle describing function corresponds to the generation of a large number of harmonics whose levels rise with the increase of the excitation σ_0. The level difference between the fundamental and the second harmonic is 29 dB for $\sigma_0 = 0.3$ but falls to 17 dB for $\sigma_0 = 0.5$, which correspond respectively to ratios of 28 and 7 between the amplitudes at the two frequencies. The contribution of this second harmonic thus cannot be neglected for large forcing amplitudes $\sigma_0 > 0.3$, in agreement with the observation made previously in figure 8. Another consequence of the highly nonlinear extended describing function is the modification of the level of the fundamental frequency, which gains 3 dB when the forcing amplitude is raised from $\sigma_0 = 0.001$ to $\sigma_0 = 0.5$. It corresponds to an increase of 40 % of the signal amplitude at this frequency. The contribution of these nonlinear effects to the modification of the time signature of the signal is visible in figure 10(*b*), especially for $t/\tau_0 = 0.75$ where the negative pressure fluctuation largely rises with the increasing value of σ_0.

4.3. *Evolution of the second-order model responses with the flow conditions*

For a harmonic excitation of frequency f_0, it has been demonstrated with (3.14) that the nonlinearities taken into account in the second-order model do not modify the amplitude of the generated wave at the fundamental frequency f_0 but generate additional noise at the first harmonic frequency $2f_0$. The non-dimensionalized amplitude of the wave at the fundamental frequency is β. The ratio between the amplitudes of the first harmonic and fundamental frequencies is $|\alpha\sigma_0/2\beta|$.

The evolution of the nozzle response at the fundamental frequency of the harmonic forcing with respect to M_1 and M_2 is represented in figure 11 for the three waves Γ_1^-, Γ_2^+ and Γ_2^-. One first observes that $\beta = 0$ when $M_1 = M_2$; with the compact nozzle assumption, this configuration corresponds to a flow in a duct of constant section where the entropy perturbation is convected without any distortion. For diverging nozzles ($M_2 < M_1$), the wave Γ_1^- is in phase and Γ_2^+ is out of phase with the forcing. The opposite is observed for converging geometries, the two waves Γ_2^+ and Γ_2^-

https://doi.org/10.1017/jfm.2013.442 Published online by Cambridge University Press

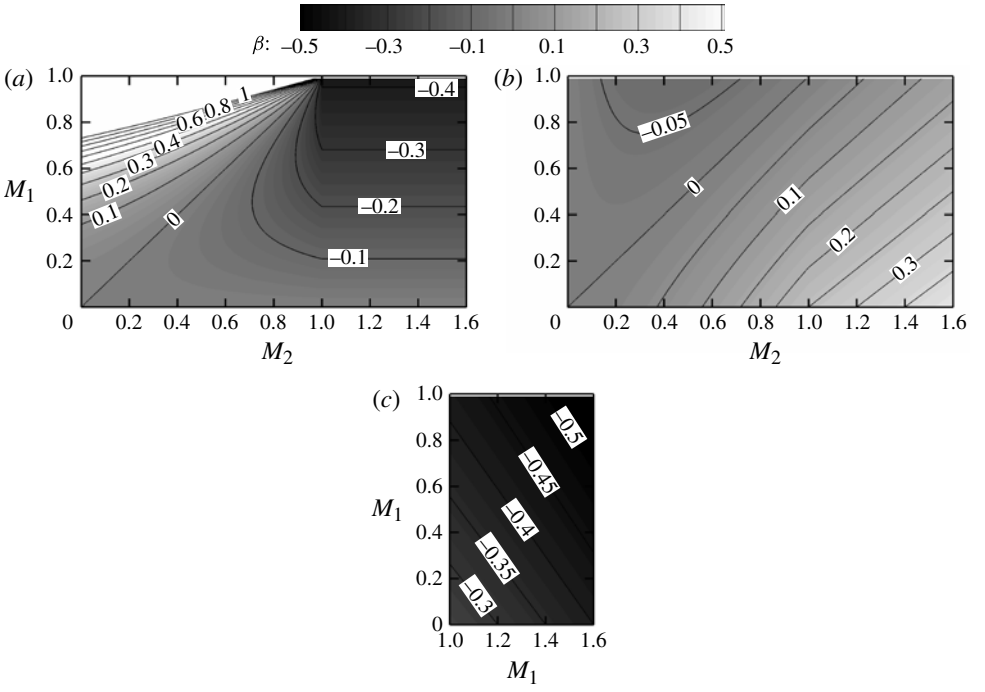


FIGURE 11. Evolution of the non-dimensional amplitude β of the acoustic waves at frequency f_0 generated by an entropy forcing at f_0 with respect to upstream (M_1) and downstream (M_2) Mach numbers for a diatomic gas ($\gamma = 1.4$): (*a*) Γ_1^-/σ; (*b*) Γ_2^+/σ; (*c*) Γ_2^-/σ.

being out of phase in the supercritical regime. More quantitatively, the amplitude of the generated waves globally holds below 0.5, which means that the characteristic acoustic waves exhibit amplitudes that are at maximum half that of the entropy forcing. An exception is visible for Γ_1^- for diverging geometries where $\beta \to +\infty$ when $M_1 \to 1$. In that case, even very small entropy perturbations can generate important acoustic fluctuations. These large fluctuations are responsible for the very limited maximum excitation amplitudes that can be used to conserve the nozzle flow regime, as discussed in § 4.1.

Previous results illustrated in figures 9 and 10 showed that the nonlinearities modify the time signature of the characteristic waves. The influence of these nonlinearities on the shape of the characteristic waves is now investigated for the second-order model. To this end, the level ratios between the first harmonic and the fundamental frequency are reproduced in figure 12 as functions of the upstream and downstream Mach numbers for the three waves. The level ratios are given for the maximum possible forcing amplitude without flow regime change, and it must be noted that these ratios are more important for lower forcings. Before discussing these results, it has to be recalled that the second-order model is accurate for all waves with the exception of Γ_1^- for diverging geometries, especially for significant values of both M_1 and M_2. Also, this level ratio only makes sense when M_1 is different from M_2. Indeed, no indirect combustion noise is generated when both Mach numbers are equal.

For subcritical configurations, the amplitude ratio for the wave Γ_2^+ lies below 0.1 for almost all Mach numbers. This wave is therefore expected to be weakly modified

https://doi.org/10.1017/jfm.2013.442 Published online by Cambridge University Press

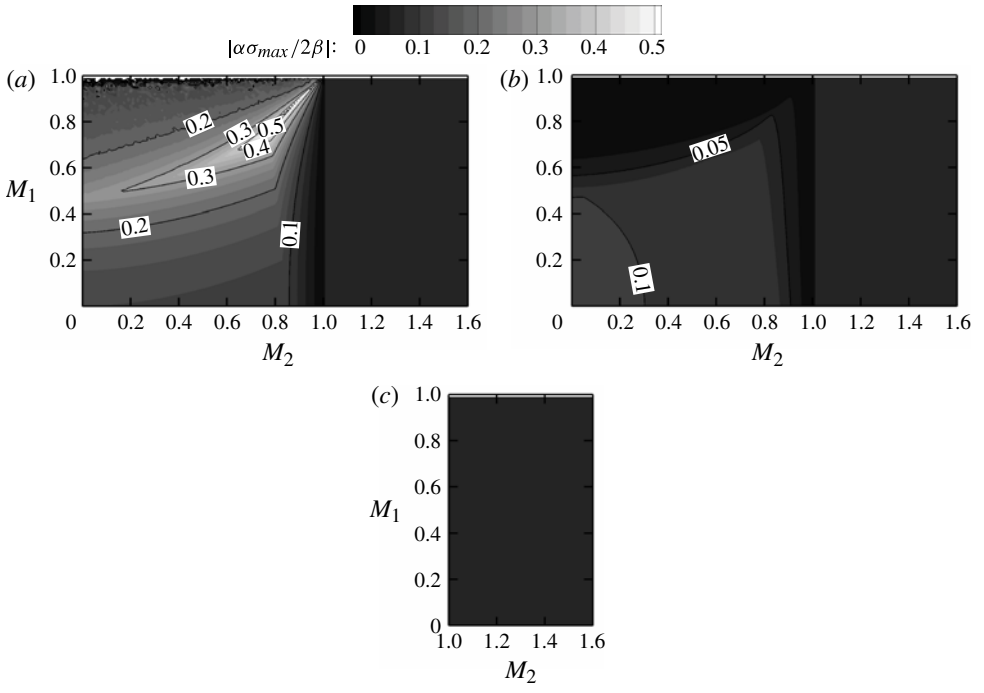


FIGURE 12. Absolute value of the amplitude ratio $|\alpha\sigma_{max}/2\beta|$ between the first harmonic ($2f_0$) and the fundamental (f_0) frequency for a harmonic entropy forcing $\sigma_{max} \leqslant 0.5$ at f_0, with respect to upstream (M_1) and downstream (M_2) Mach numbers for a diatomic gas ($\gamma = 1.4$): (*a*) Γ_1^-/σ; (*b*) Γ_2^+/σ; (*c*) Γ_2^-/σ.

by the nonlinearities in the presence of large entropy forcings. This level ratio rises to 0.25 for Γ_1^- for converging geometries. The shape modification of the wave is thus expected to be more visible in that case. Finally, the highest-amplitude ratio of 0.5 is obtained for high subsonic values of both M_1 and M_2. For these flow configurations, nevertheless, the error of the second-order model rises above 70 %, which indicates that the second-order model fails to correctly predict the acoustic generated.

For supercritical nozzles, the ratio $|\alpha\sigma/2\beta| = |\sigma|/8$ is independent of the upstream and downstream Mach numbers and of the adiabatic coefficient γ, for all three waves. The amplitude difference between the two frequencies therefore only depends on the forcing amplitude and the level of the harmonic is negligible compared to the one at the fundamental frequency, the ratio being $1/16$ for $\sigma = 0.5$.

To conclude, one can note the high correlation between the relative level of the first-order harmonic predicted by the second-order model and the error of the second-order model, in figure 6: the lower the difference between the first harmonic and fundamental frequencies predicted by the second-order model, the higher the error of the model compared to the full nonlinear solution. It indicates that modelling the generation of large nonlinear waves cannot be performed with second-order perturbative terms alone. In that case, higher-order perturbations are not negligible and have to be taken into account. In the spectral domain, the nonlinearities of the generated waves are therefore not limited to the first harmonic but correspond to the generation of important noise levels for a large number of harmonic frequencies, as has been observed in figures 8 and 9(*b*).

https://doi.org/10.1017/jfm.2013.442 Published online by Cambridge University Press

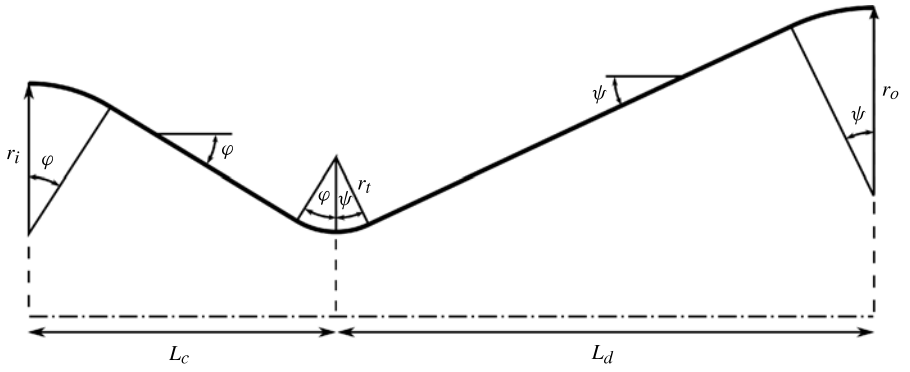


FIGURE 13. General shape of the nozzle geometry proposed by Sigman & Zinn (1983).

		M_1	M_2	L_c (m)	L_d (m)	r_i (m)	r_t (m)	r_o (m)	Ω_0
Case 1	Supercritical nozzle	0.1	1.3	0.010	0.030	0.002	0.002	0.002	0.058
Case 2	Converging nozzle	0.1	0.3	0.015	—	0.002	0.002	—	0.070
Case 3	Diverging nozzle	0.5	0.2	—	0.030	—	0.002	0.002	0.074

TABLE 5. Nozzle characteristics and flow conditions. The compactness criterion Ω_0 is evaluated at the forcing frequency $f_0 = 40$ Hz.

5. Validation of the analytical solutions

In this section, the analytical extended nozzle describing functions are validated by means of comparisons with numerical simulations in the subcritical and supercritical flow regimes. Computations are performed with the code Sunday, described in § 2.3.

In order to study nozzles of realistic shapes, the geometries considered here correspond to the nozzle shape proposed by Sigman & Zinn (1983) and illustrated in figure 13. Both in the converging and the diverging parts, the section radius evolves linearly with the axial distance. A circular shape is used to smooth the transition at the throat, the nozzle inlet and the nozzle outlet. The definition of the inlet, outlet and throat Mach numbers, the circle radii at the inlet, outlet and nozzle throat (r_i, r_o, r_t), and the convergence and divergence angles (φ, ψ) or converging and diverging section lengths (L_c, L_d) are sufficient to design any nozzle of this family, allowing investigation of a wide range of flows from subsonic to supersonic. Nozzle characteristics for the simulated cases are summarized in table 5.

The non-reflective boundary conditions used for the simulations (Navier–Stokes characteristic boundary conditions) rely on the separation of acoustic, entropy and vorticity waves at the domain inlet and outlet, in the linear domain (Poinsot & Lele 1992). In the present study, entropy perturbations can be as large as $\sigma = 0.5$ and may lead to large generated acoustic waves p'/p_0. To avoid any spurious noise generation at the inlet and outlet due to the interaction of high-amplitude entropy or acoustic waves with the boundary conditions, damping zones are added upstream and downstream of the nozzle region using a grid stretching of 2 % to attenuate the waves before they reach the domain boundaries.

https://doi.org/10.1017/jfm.2013.442 Published online by Cambridge University Press

The simulations are performed using nonlinear perturbation equations for thermodynamically perfect air, meaning that the heat capacity c_p is independent of the temperature. Validations of the nonlinear compact model are performed for three separate operating conditions, namely a supercritical nozzle, a subcritical converging nozzle and a subcritical diverging nozzle. Flow characteristics for the three regimes are summarized in table 5. All simulations are performed with the same inlet temperature $T_{inlet} = 300$ K and outlet pressure $p_{outlet} = 101\,325$ Pa. The entropy perturbation is spatially superimposed upstream of the nozzle inlet at the beginning of the simulations through the perturbed flow fields ρ', u' and p'. The fluctuation is harmonic and defined over one wavelength, with an amplitude of $\sigma_0 = 0.5$. The fluctuation is, moreover, assumed to be isobaric, $p' = 0$, and the density fluctuation is deduced from the entropy relation. The initial perturbed flow fields are therefore given by

$$\rho' = \mathrm{e}^{-\sigma} - 1, \tag{5.1}$$

$$u' = 0, \tag{5.2}$$

$$p' = 0. \tag{5.3}$$

As mentioned above, constant section duct regions are included in the numerical grid at the left and right sides of the nozzle. The acoustic waves generated in the nozzle thus pass through the temperature inhomogeneity in those duct sections and interact with it, part of the waves being reflected and going back to the nozzle where they generate additional noise in the upstream and downstream directions (Candel, Defillipi & Launay 1980), as illustrated in figure 14. These wave reflections can be neglected for a small-amplitude entropy perturbation but may become noticeable when the temperature fluctuation amplitude increases. To compare the noise generated by the entropy fluctuation in the simulations with the analytical solutions, the contributions resulting from the incident acoustic waves are subtracted from the characteristic waves evaluated upstream and downstream of the nozzle in the simulations using (2.10). Therefore, in this section all the characteristic waves reproduced are solely the result of the entropy forcing and do not include any acoustic contribution. The method used to extract the entropy contribution from the generated noise is illustrated in figure 14, which represents the different waves present in the simulations and their origin for the subcritical regime. The entropy forcing generates the two waves Γ_{1e}^- and Γ_{2e}^+. Their interaction with the large-amplitude entropy perturbation creates the waves Γ_1^+ and Γ_2^-, which go back to the nozzle and generate the additional waves Γ_{1a}^- and Γ_{2a}^+. These waves are expected to be small, though non-negligible, compared to Γ_{1e}^- and Γ_{2e}^+ and their interaction with the entropy wave is neglected. The outcoming acoustic characteristics are therefore denoted by $\left(\Gamma_{1e}^- + \Gamma_{1a}^-\right)$ and $\left(\Gamma_{2e}^+ + \Gamma_{2a}^+\right)$, respectively upstream and downstream of the nozzle. In practice, the evaluation of the characteristic waves at the end of the numerical simulation provides the amplitudes of the outcoming waves $\left(\Gamma_{1e}^- + \Gamma_{1a}^-\right)$ and $\left(\Gamma_{2e}^+ + \Gamma_{2a}^+\right)$ and incoming acoustic waves Γ_1^+ and Γ_2^-. The waves Γ_{1a}^- and Γ_{2a}^+ are then determined using the incoming acoustic waves and the analytical models. Subtracting these waves from the outcoming waves finally provides the contribution of the entropy perturbation to the acoustic waves, Γ_{1e}^- and Γ_{2e}^+.

Nonlinear interactions between acoustic and entropy waves may also occur for the convection of the entropy wave. The acoustic velocity fluctuations upstream of the nozzle can be expected to be large enough to be non-negligible compared to the mean velocity, and might consequently modify the shape of the convected entropy perturbation. To provide accurate theoretical solutions, the analytical signals

https://doi.org/10.1017/jfm.2013.442 Published online by Cambridge University Press

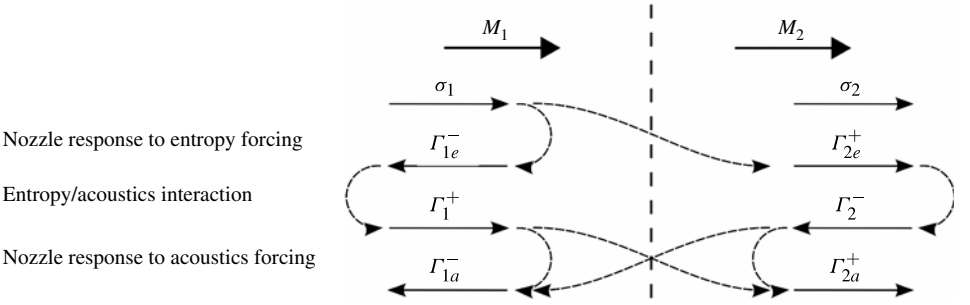


FIGURE 14. Interaction between entropy and acoustic waves upstream and downstream of a subsonic compact nozzle.

are determined using the entropy fluctuations computed at the nozzle inlet using Sunday.

Finally, to ensure the nozzle compactness for all simulated configurations, the compactness criterion $\Omega_0 = \omega_0 \times \int_0^L \mathrm{d}\xi/u(\xi)$, where $\omega_0 = 2\pi f_0$ is the angular frequency of the forcing signal and L the axial length of the nozzle, has been calculated and is reported in table 5. This criterion was initially proposed by Giauque *et al.* (2012) and represents the ratio between the time needed by the entropy wave to pass through the nozzle and its period $\tau_0 = 1/f_0$. Its low value indicates that the fluctuation can indeed be considered constant through the entire nozzle, so that the nozzle appears to be compact even for frequencies several times larger than f_0. This last result is especially important because the inlet forcing signals are not necessarily harmonic in the simulations because of the distortions occurring during their convection to the nozzle entrance. This compactness criterion result has moreover been validated by simulations of the linear nozzle transfer functions.

5.1. *Case 1: supercritical nozzle*

The first validation is performed for the supercritical nozzle, where the flow is accelerated from $M_1 = 0.1$ to $M_2 = 1.3$. The entropy signal at the nozzle inlet is reproduced in figure 15 and compared to a harmonic forcing. The modification of the signal shape by its interaction with the upstream acoustic wave is clearly visible in the figure and can be explained qualitatively using the linear model. Using (4.2), the velocity perturbation upstream of the nozzle is given by $u_1'/u_1 = -\beta\sigma/M_1$ with $\beta/M_1 = -0.49$ in the present configuration. The flow velocity is therefore increased for a positive entropy forcing and decreased for a negative one. For a forcing of amplitude $\sigma = 0.5$, the perturbed velocity amplitude is $\sim$25 % of the mean velocity, which explains the visible shape modification of the entropy signal at the nozzle inlet.

The time signatures obtained with Sunday for the three characteristic waves are represented in figure 16 and are compared with the analytical models. Very good agreement is observed between the simulated signals and the full nonlinear solutions both upstream and downstream of the nozzle. The second-order model solutions also agree with the simulated time signatures thanks to the very low discrepancy of this model with the full nonlinear solution, which is 1 % for all waves. More important differences are observed between the first-order model and the simulated signals. This last result especially illustrates the contribution of the first harmonic frequency to the time signatures for the noise generated with this nonlinear entropy forcing, which is not taken into account with the linear model. For the present supercritical

https://doi.org/10.1017/jfm.2013.442 Published online by Cambridge University Press

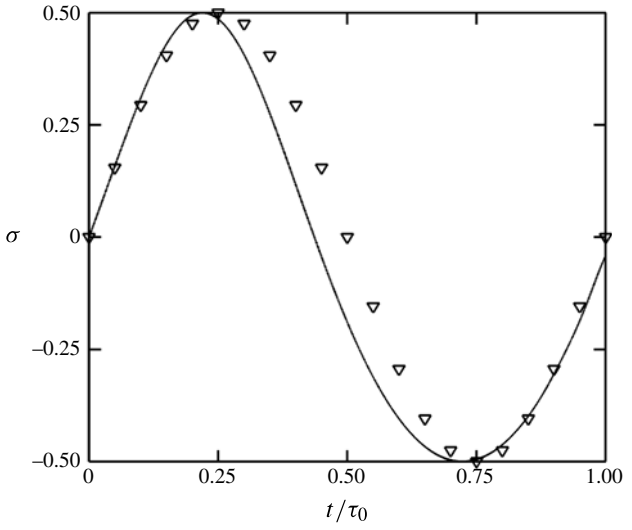


FIGURE 15. Entropy signal at nozzle inlet: −, Sunday; ▽, analytical harmonic forcing. Supercritical configuration.

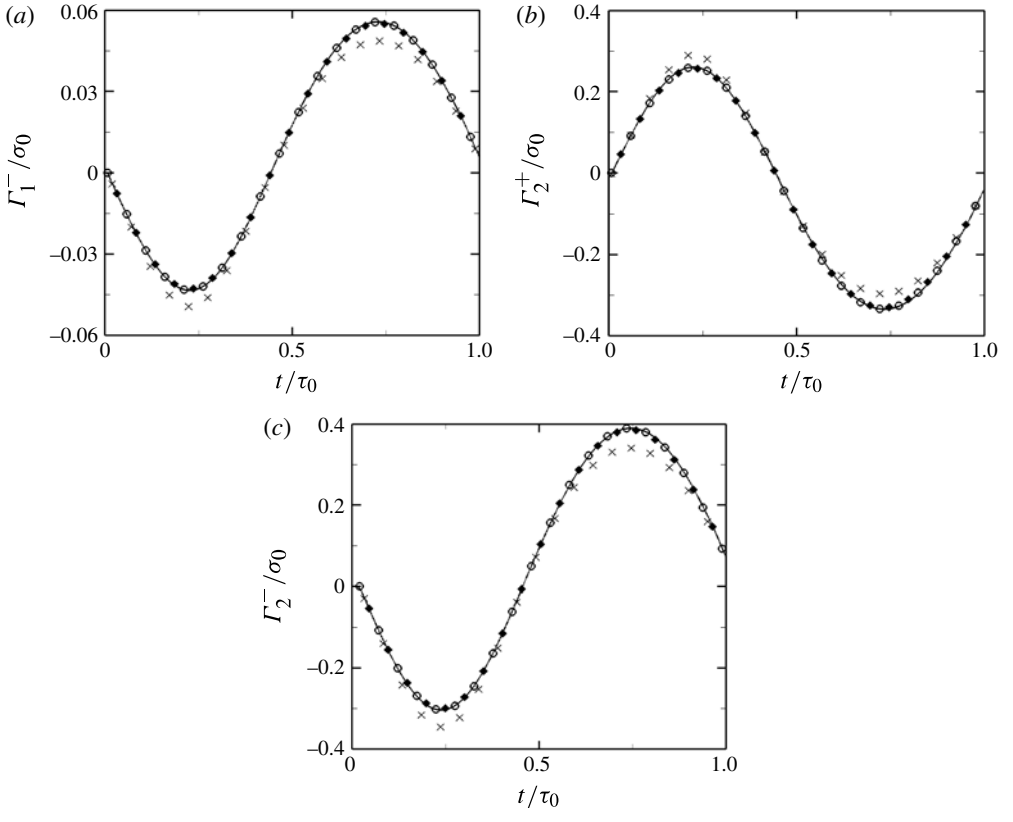


FIGURE 16. Characteristic wave fluctuations (*a*) at nozzle inlet and nozzle outlet for (*b*) downstream and (*c*) upstream acoustic waves: −, Sunday; ×, first-order model (Marble & Candel 1977); ♦, second-order model; ∘, full nonlinear model. Supercritical configuration. (*a*) Γ_1^-; (*b*) Γ_2^+; (*c*) Γ_2^-.

https://doi.org/10.1017/jfm.2013.442 Published online by Cambridge University Press

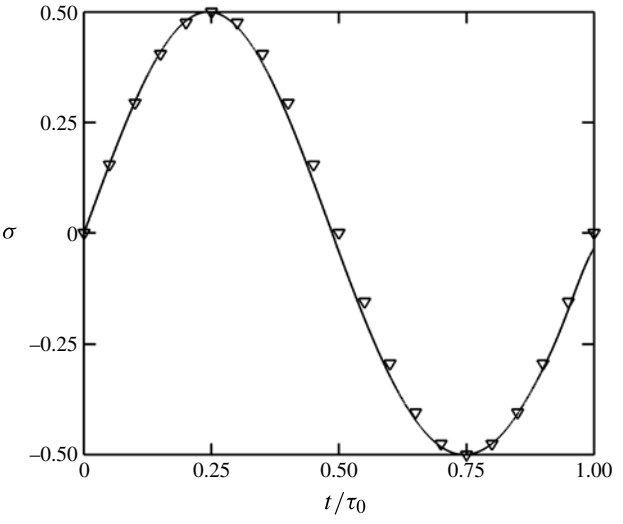


FIGURE 17. Entropy signal at nozzle inlet: −, Sunday; ▽, analytical harmonic forcing. Subcritical converging nozzle configuration.

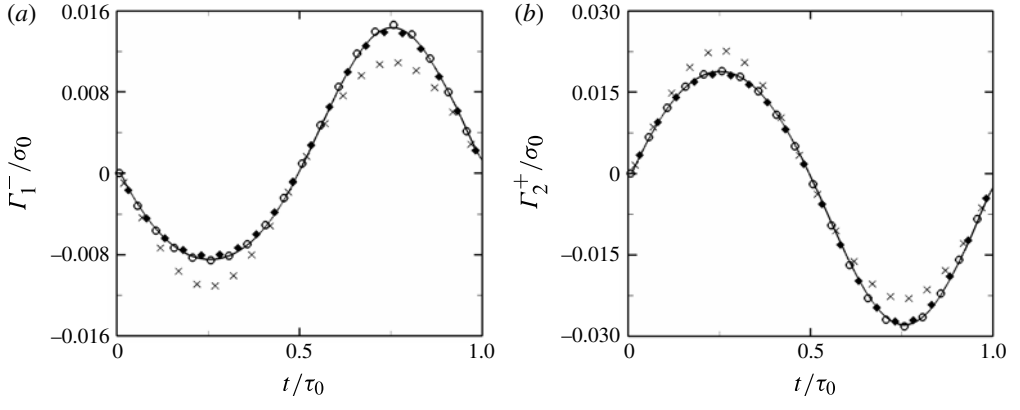


FIGURE 18. Characteristic wave fluctuations (*a*) at nozzle inlet and (*b*) nozzle outlet: −, Sunday; ×, first-order model (Marble & Candel 1977); ♦, second-order model; ∘, full nonlinear model. Subcritical converging nozzle configuration. (*a*) Γ_1^-; (*b*) Γ_2^+.

configuration, the results of § 4.3 indicate that the amplitude ratio between the first harmonic and fundamental frequencies is 0.06.

5.2. *Case 2: subcritical converging nozzle*

The second validation corresponds to the subcritical converging nozzle with $M_1 = 0.1$ and $M_2 = 0.3$. For this configuration, the coefficient driving the upstream velocity perturbation in the linear domain is $\beta/M_1 = -0.11$, a value five times smaller than that of the supercritical configuration above. Similar but weaker modifications of the entropy signal shape are therefore expected at the nozzle inlet, as confirmed in figure 17.

The simulated characteristic waves are compared to the full nonlinear solutions in figure 18. The analytical solutions reproduce very well the numerical results of the

https://doi.org/10.1017/jfm.2013.442 Published online by Cambridge University Press

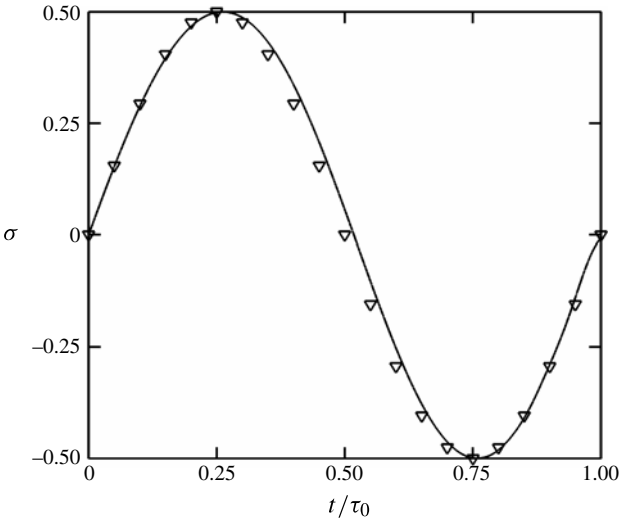


FIGURE 19. Entropy signal at nozzle inlet: −, Sunday; ▽, analytical harmonic forcing. Subcritical diverging nozzle configuration.

code Sunday. The relative error of the second-order model is 5 % for Γ_1^- and 2.9 % for Γ_2^+. This discrepancy is higher than that observed for the supercritical nozzle but remains sufficiently low for the analytical solutions to collapse. As the analytical amplitude ratios between the first harmonic and the fundamental frequencies are 0.13 for Γ_1^- and 0.10 for Γ_2^+, the discrepancies observed for the linear model are more pronounced than for the previous supercritical configuration.

5.3. *Case 3: subcritical diverging nozzle*

The last validation of the paper is a subcritical diverging nozzle with $M_1 = 0.5$ and $M_2 = 0.2$. The upstream velocity fluctuation predicted by the linear analysis is related to $\beta/M_1 = 0.29$, so the local velocity decreases for positive forcings and increases for negative forcings. As is visible in figure 19, the simulation verifies this predicted modification of the entropy signal shape. The time signature distortion nevertheless seems lower than that expected with the large value of β/M_1. It must be recalled that, for this configuration, the analyses performed in § 4 demonstrated the highly nonlinear nozzle response to large entropy forcings for the upstream acoustic wave. The linear analysis therefore cannot predict quantitatively the shape modification of the entropy signal.

Figure 20 reproduces the characteristic waves obtained with the simulation and the analytical models. The full nonlinear model agrees with the signals computed with Sunday for both Γ_1^- and Γ_2^+. The second-order model signal also agrees with the computed signal downstream of the nozzle. The discrepancy between the two models for this wave is 1.5 %. In the upstream direction, the relative error between the two analytical solutions rises to 45 % and the second-order model strongly underestimates the amplitude of the computed generated wave. The discrepancy is even more pronounced for the linear model. The error is especially visible for $t/\tau_0 \sim 0.75$, where the underprediction reaches 60 % for the first-order solution.

https://doi.org/10.1017/jfm.2013.442 Published online by Cambridge University Press

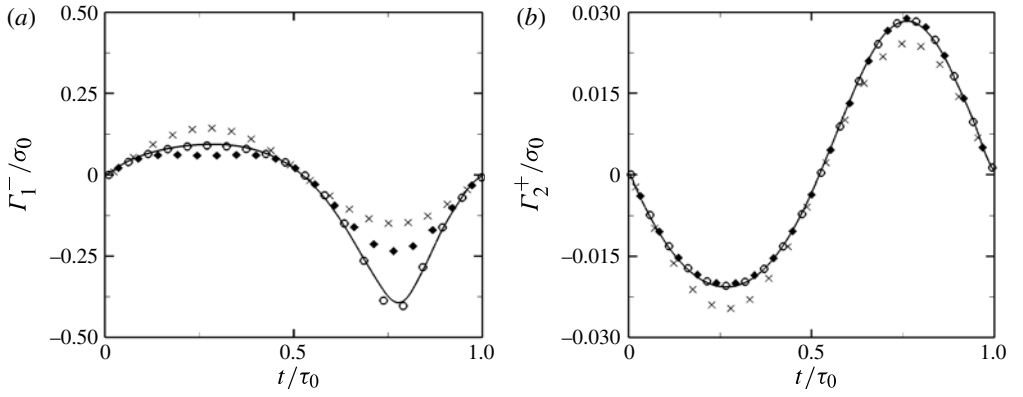


FIGURE 20. Characteristic wave fluctuations (*a*) at nozzle inlet and (*b*) nozzle outlet: −, Sunday; ×, first-order model (Marble & Candel 1977); ♦, second-order model; ∘, full nonlinear model. Subcritical diverging nozzle configuration. (*a*) Γ_1^-; (*b*) Γ_2^+.

6. Conclusion

Below a few hundred Hz, entropy waves have wavelengths that become comparable to the turbulent integral scale in the engine and may not be subject to damping. Since they have moreover been shown recently to be a key ingredient in the onset or sustainability of some combustion instabilities (Giauque 2007; Brear *et al.* 2012; Motheau *et al.* 2013), it is legitimate to consider that their amplitude might be large enough to lie in the nonlinear domain (typically above 100 K for a 1000 K averaged background temperature in the combustion chamber).

To study the indirect combustion noise generated by such low-frequency, nonlinear excitations, the analytical model of Marble and Candel for compact nozzles (Marble & Candel 1977) initially developed for excitations in the linear regime is rederived and extended to the nonlinear domain. Both subcritical and supercritical nozzles in the absence of shock are considered. A detailed methodology for the resolution of the nonlinear systems is provided. The amplitudes of the generated acoustic waves $\Gamma^{\pm}$ with respect to the amplitude of the acoustic or entropy excitation are discussed. As a way of simplifying and further analysing the nonlinear response of the nozzle to large-amplitude entropy excitations, a second-order model is proposed. Its accuracy is carefully analysed by varying the inlet and outlet Mach numbers of the nozzle. One observes that the second-order model is very accurate in the supercritical regime regardless of the type of wave considered, with the error being of 1 %. In the subcritical regime, the error is negligible for Γ_2^+ for all Mach numbers and remains low for Γ_1^- for almost all converging geometries. For those configurations, the flow nonlinearities therefore essentially lead to the generation of additional noise at the first harmonic of the forcing frequency. The error is more important for Γ_1^- for diverging nozzles, especially for significant values of M_1 and M_2 where the discrepancy between second-order and full nonlinear solutions rises above 70 %. For these geometries, contributions of high-order nonlinearities occur in the flow and may lead to important modifications of the generated acoustic wave Γ_1^- compared to the linear regime. In this comparison process, it is also shown that the first-order solution is the exact solution of the full nonlinear equations in the case of a supercritical nozzle subject to incoming nonlinear acoustic waves.

https://doi.org/10.1017/jfm.2013.442 Published online by Cambridge University Press

In the context of indirect combustion noise, the phenomenon of regime change of the nozzle due to an incoming entropy fluctuation is also addressed. These changes of regime are related to the modifications of the Mach number induced by temperature and velocity fluctuations. This phenomenon translates in the context of the present study into a limitation of the maximum amplitude of the incoming entropy forcing. Limitations of this kind are to be considered for subcritical nozzles with significant inlet or outlet Mach numbers, where the flow transition is observed even for very low-amplitude entropy excitations. With the constraint of those limitations, the extended nozzle describing functions representing the full nonlinear response for indirect combustion noise are validated through detailed comparisons with numerical simulations in the subcritical and supercritical flow regimes.

Acknowledgement

The authors would like to acknowledge the support of their work by MAMBO, the ONERA internal research initiative for combustion noise.

Appendix. Expression of the conservation equations in perturbative form

In this appendix the conservation equations are written in the perturbative form for the natural variables. For a subcritical nozzle, the three conserved quantities are the mass flow rate, the stagnation temperature and the entropy. Following the terminology used in the paper, they are given by

$$\dot{m} = \rho u A, \tag{A 1}$$

$$T_t = T\left(1 + \frac{\gamma - 1}{2} M^2\right), \tag{A 2}$$

$$s = c_p \ln \frac{p^{1/\gamma}}{\rho}. \tag{A 3}$$

Let us express the perturbed flow variables in the form $z_0\,(1 + z'/z_0)$, where z stands for any variable ρ, $p, \ldots$. Assuming an ideal gas, (A 1)–(A 2) can be expressed as follows in perturbative form, after some algebra:

$$1 + \frac{\dot{m}'}{\dot{m}_0} = \left(1 + \frac{u'}{u_0}\right)\left(1 + \frac{p'}{p_0}\right)^{1/\gamma} \mathrm{e}^{-s'/c_p}, \tag{A 4}$$

$$1 + \frac{T_t'}{T_{t0}} = \frac{1}{1 + \dfrac{\gamma - 1}{2} M_0^2}\left(\left(1 + \frac{p'}{p_0}\right)^{(\gamma-1)/\gamma} \mathrm{e}^{s'/c_p} + \frac{\gamma - 1}{2} M_0^2 \left(1 + \frac{u'}{u_0}\right)^2\right). \tag{A 5}$$

In the supercritical regime, the mass flow rate is imposed by the flow upstream of the nozzle throat. It is referred to as the critical mass flow rate $\dot{m}_\star$ and can be expressed as a function of stagnation pressure p_t and temperature T_t only (Landau & Lifshitz 1966), or, similarly, as a function of static pressure, static temperature and Mach number,

$$\begin{aligned}\dot{m}_\star &= A_\star p_t \sqrt{\frac{\gamma}{r T_t}}\left(\frac{\gamma + 1}{2}\right)^{-(\gamma+1)/2(\gamma-1)} \\ &= A_\star \sqrt{\frac{\gamma}{r}}\left(\frac{\gamma + 1}{2}\right)^{-(\gamma+1)/2(\gamma-1)} \frac{p}{\sqrt{T}}\left(1 + \frac{\gamma - 1}{2} M^2\right)^{(\gamma+1)/2(\gamma-1)}\end{aligned} \tag{A 6}$$

https://doi.org/10.1017/jfm.2013.442 Published online by Cambridge University Press

with $A_\star$ the surface section at the nozzle throat, where $M_\star = 1$. In perturbative form, the critical mass flow rate fluctuation is given by

$$1 + \frac{\dot{m}'_\star}{\dot{m}_{\star 0}} = \left(1 + \frac{p'}{p_0}\right)^{(\gamma+1)/2\gamma} \mathrm{e}^{-s'/2c_p} \times \left(1 + \frac{\dfrac{\gamma-1}{2}M_0^2}{1 + \dfrac{\gamma-1}{2}M_0^2}\left(-1 + \left(1 + \frac{u'}{u_0}\right)^2 \left(1 + \frac{p'}{p_0}\right)^{-(\gamma-1)/\gamma} \mathrm{e}^{-s'/c_p}\right)\right)^{(\gamma+1)/2(\gamma-1)}. \tag{A 7}$$

Both (A 4) and (A 7) express the fluctuations of the mass flow rate. By combining the two expressions, one finally obtains the following equation, which holds both upstream and downstream of the nozzle

$$0 = \left(1 + \frac{p'}{p_0}\right)^{(\gamma-1)/2\gamma} \left(1 + \frac{u'}{u_0}\right)^{-1} \mathrm{e}^{s'/2c_p} \times \left[1 + \frac{\dfrac{\gamma-1}{2}M_0^2}{1 + \dfrac{\gamma-1}{2}M_0^2}\left(-1 + \left(1 + \frac{u'}{u_0}\right)^2 \left(1 + \frac{p'}{p_0}\right)^{-(\gamma-1)/\gamma} \mathrm{e}^{-s'/c_p}\right)\right]^{(\gamma+1)/2(\gamma-1)} - 1. \tag{A 8}$$

REFERENCES

ACARE 2010 Aeronautics and air transport: beyond vision 2020 (towards 2050). European Union.

ATASSI, O. V. & GILSON, J. J. 2010 Acoustic mode scattering from a heat source. *J. Fluid Mech.* **651**, 1–26.

BAKE, F., KINGS, N., FISCHER, A. & RÖHLE, I. 2009 Experimental investigation of the entropy noise mechanism in aero-engines. *Intl J. Aeroacoust.* **8**, 125–142.

BERLAND, J., BOGEY, C., MARSDEN, O. & BAILLY, C. 2007 High-order, low dispersive and low dissipative explicit schemes for multiple-scale and boundary problems. *J. Comput. Phys.* **224**, 637–662.

BEYER, R. T. 1997 *Nonlinear Acoustics*. Acoustical Society of America.

BLOY, A. W. 1979 The pressure waves produced by the convection of temperature disturbances in high subsonic nozzle flows. *J. Fluid Mech.* **93**, 465–475.

BOGEY, C. & BAILLY, C. 2004 A family of low dispersive and low dissipative explicit schemes for flow and noise computations. *J. Comput. Phys.* **194**, 194–214.

BOHN, M. S. 1977 Response of a subsonic nozzle to acoustic and entropy disturbances. *J. Sound Vib.* **52**, 283–297.

BOUDIER, G., LAMARQUE, N., STAFFELBACH, G., GICQUEL, L. Y. M. & POINSOT, T. 2009 Thermo-acoustic stability of a helicopter gas turbine combustor using large-eddy simulations. *Intl J. Aeroacoust.* **8**, 69–94.

BREAR, M. J., NICOUD, F., TALEI, M., GIAUQUE, A. & HAWKES, E. R. 2012 Disturbance energy transport and sound production in gaseous combustion. *J. Fluid Mech.* **707**, 53–73.

DE CACQUERAY, N. 2010 Méthodes numériques pour les écoulements supersoniques avec application au calcul du bruit rayonné par un jet sur-détendu. PhD thesis, École Centrale de Lyon, Lyon, France.

CANDEL, S. M. 1972 Analytical studies of some acoustic problems of jet engines. PhD thesis, California Institute of Technology, Pasadena.

https://doi.org/10.1017/jfm.2013.442 Published online by Cambridge University Press

CANDEL, S. M., DEFILLIPI, F. & LAUNAY, A. 1980 Determination of the inhomogeneous structure of a medium from its plane wave reflection response. Part 1. A numerical analysis of the direct problem. *J. Sound Vib.* **68**, 571–582.

CANDEL, S. M., DUROX, D., SCHULLER, T., PALIES, P., BOURGOUIN, J.-F. & MOECK, J. P. 2012 Progress and challenges in swirling flame dynamics. *Comptes Rendus Mécanique* **340**, 758–768.

CUMPSTY, N. A. & MARBLE, F. E. 1977 The interaction of entropy fluctuations with turbine blade rows: a mechanism of turbojet engine noise. *Proc. R. Soc. Lond.* A **357**, 323–344.

DURÁN, I., LEYKO, M., MOREAU, S., NICOUD, F. & POINSOT, T. 2013*a* Computing combustion noise by combining large eddy simulations with analytical models for the propagation of waves through turbine blades. *Comptes Rendus Mécanique* **341**, 131–140.

DURÁN, I. & MOREAU, S. 2013 Solution of the quasi-one-dimensional linearized Euler equations using flow invariants and the Magnus expansion. *J. Fluid Mech.* **723**, 190–231.

DURÁN, I., MOREAU, S. & POINSOT, T. 2013*b* Analytical and numerical study of combustion noise through a subsonic nozzle. *AIAA J.* **51**, 42–52.

GIAUQUE, A. 2007 Fonctions de transfert de flamme et énergies de perturbation dans les écoulements réactifs. PhD thesis, Institut National Polytechnique de Toulouse, Toulouse, France.

GIAUQUE, A., HUET, M. & CLERO, F. 2012 Analytical analysis of indirect combustion noise in subcritical nozzles. *Trans. ASME: J. Engng Gas Turbines Power* **134**, 111202.

GOH, C. S. & MORGANS, A. S. 2011 Phase prediction of the response of choked nozzles to entropy and acoustic disturbances. *J. Sound Vib.* **330**, 5184–5198.

GOH, C. S. & MORGANS, A. S. 2013 The influence of entropy waves on the thermoacoustic stability of a model combustor. *Combust. Sci. Technol.* **185**, 249–268.

HOCHGREB, S., DENNIS, D., AYRANCI, I., BAINBRIDGE, W. & CANT, S. 2013 Forced and self-excited instabilities from lean premixed, liquid-fuelled aeroengine injectors at high pressures and temperatures. In *Proceedings of ASME Turbo Expo, Paper* GT2013-95311.

HOWE, M. S. 2010 Indirect combustion noise. *J. Fluid Mech.* **659**, 267–288.

KAUFMANN, A., NICOUD, F. & POINSOT, T. 2002 Flow forcing techniques for numerical simulation of combustion instabilities. *Combust. Flame* **131**, 371–385.

LANDAU, L. D. & LIFSHITZ, E. M. 1966 *Course of Theoretical Physics, vol. 6: Fluid Mechanics*, 3rd edn. Pergamon Press.

LEYKO, M., MOREAU, S., NICOUD, F. & POINSOT, T. 2010 Waves transmission and generation in turbine stages in a combustion–noise framework. In *16th AIAA/CEAS Aeroacoustics Conference, AIAA Paper* 2010-4032.

LEYKO, M., MOREAU, S., NICOUD, F. & POINSOT, T. 2011 Numerical and analytical modelling of entropy noise in a supersonic nozzle with a shock. *J. Sound Vib.* **330**, 3944–3958.

MARBLE, F. E. 1973 Acoustic disturbance from gas non-uniformities convecting through a nozzle. In *Interagency Symposium on University Research in Transportation Noise, Stanford University, Stanford, CA*, pp. 547–561.

MARBLE, F. E. & CANDEL, S. M. 1977 Acoustic disturbance from gas non-uniformities convected through a nozzle. *J. Sound Vib.* **55**, 225–243.

MISHRA, A. & BODONY, D. J. 2013 Evaluation of actuator disk theory for predicting indirect combustion noise. *J. Sound Vib.* **332**, 821–838.

MOASE, W. H., BREAR, M. J. & MANZIE, C. 2007 The forced response of choked nozzles and supersonic diffusers. *J. Fluid Mech.* **585**, 281–304.

MORFEY, C. L. 1973 Amplification of aerodynamic noise by convected flow inhomogeneities. *J. Sound Vib.* **31**, 391–397.

MOTHEAU, E., NICOUD, F., MERY, Y. & POINSOT, T. 2013 Analysis and modelling of entropy modes in a realistic aeronautical gas turbine. In *Proceedings of ASME Turbo Expo, Paper* GT2013-94224.

MÜHLBAUER, B., NOLL, B. & AIGNER, M. 2009 Numerical investigation of the fundamental mechanism for entropy noise generation in aero-engines. *Acta Acust. United With Acustica* **95**, 470–478.

https://doi.org/10.1017/jfm.2013.442 Published online by Cambridge University Press

NOIRAY, N., DUROX, D., SCHULLER, T. & CANDEL, S. 2008 A unified framework for nonlinear combustion instability analysis based on the flame describing function. *J. Fluid Mech.* **615**, 139–167.

PASCHEREIT, C. O., SCHUERMANS, B., POLIFKE, W. & MATTSON, O. 2002 Measurement of transfer matrices and source terms of premixed flames. *Trans. ASME: J. Engng Gas Turbines Power* **124**, 239–247.

POINSOT, T. J. & LELE, S. K. 1992 Boundary conditions for direct simulations of compressible viscous flows. *J. Comput. Phys.* **101**, 104–129.

SIGMAN, R. K. & ZINN, B. T. 1983 A finite element approach for predicting nozzle admittances. *J. Sound Vib.* **88**, 117–131.

STEIN, W. & JOYNER, D. 2005 SAGE: system for algebra and geometry experimentation. *ACM SIGSAM Bulletin* **39**, 61–64.

STOW, S. R., DOWLING, A. P. & HYNES, T. P. 2002 Reflection of circumferential modes in a choked nozzle. *J. Fluid Mech.* **467**, 215–239.

THOMPSON, K. W. 1987 Time dependent boundary conditions for hyperbolic systems. *J. Comput. Phys.* **68**, 1–24.

THOMPSON, K. W. 1990 Time dependent boundary conditions for hyperbolic systems. Part 2. *J. Comput. Phys.* **89**, 439–461.

WOLF, P., BALAKRISHNAN, R., STAFFELBACH, G., GICQUEL, L. Y. M. & POINSOT, T. 2012 Using LES to study reacting flows and instabilities in annular combustion chambers. *Flow Turbul. Combust.* **88**, 191–206.

https://doi.org/10.1017/jfm.2013.442 Published online by Cambridge University Press